

Tight-binding theory of spin-orbit coupling in graphynes

Guido van Miert, Vladimir Juričić, and Cristiane Morais Smith
*Institute for Theoretical Physics, Centre for Extreme Matter and Emergent Phenomena,
Utrecht University, Leuvenlaan 4, 3584 CE Utrecht, The Netherlands*

We investigate the effects of Rashba and intrinsic spin-orbit couplings (SOC) in graphynes. First, we develop a general method to address spin-orbit couplings within the tight-binding theory. Then, we apply this method to α -, β -, and γ -graphyne, and determine the SOC parameters in terms of the microscopic hopping and on-site energies. We find that for α -graphyne, as in graphene, the intrinsic SOC opens a non-trivial gap, whereas the Rashba SOC splits each Dirac cone into four. In β - and γ -graphyne, the Rashba SOC can lead to a Lifshitz phase transition, thus transforming the zero-gap semiconductor into a gapped system or vice versa, when pairs of Dirac cones annihilate or emerge. The existence of internal (within the benzene ring) and external SOC in these compounds allows us to explore a myriad of phases not available in graphene.

PACS numbers: 73.22.-f, 81.05.Zx, 31.15.aj, 31.15.ae

I. INTRODUCTION

During the last decade, graphene has attracted enormous attention, and has provided a new paradigm for studying pseudo-relativistic fermions in condensed-matter systems [1]. The peculiar Dirac-type structure of its low-energy quasiparticles arises due to the lattice geometry and time-reversal symmetry. The honeycomb lattice, which consists of two equivalent interpenetrating triangular lattices, gives rise to the touching of the valence and conduction bands at two inequivalent K and K' points at the corners of the hexagonal Brillouin zone (BZ), which are related by time-reversal symmetry. Although the first proposal for a time-reversal topological insulator invoked graphene [2], its experimental realization has been hampered by the weak spin-orbit coupling (SOC) in this material. On the other hand, this created a lot of activity towards the tailoring of artificial structures exhibiting Dirac cones and strong SOC. Some of the so far proposed systems include self-assembled honeycomb arrays of CdSe and PbSe semiconducting nanocrystals [3], patterned quantum dots [4], and molecular graphene [5]. Yet another interesting class of Dirac materials in this respect consists of graphynes.

Graphynes are two-dimensional carbon allotropes that differ from graphene by the presence of triple bonds ($-C \equiv C-$) into their lattice structure [6]. Figure 1 displays the lattice structure of α -, β -, and γ -graphyne. They have not been experimentally realized yet, as opposed to graphdiyne [7], which features *pairs* of acetylene bonds in its crystal lattice. Since their proposal in 1987 [8], they have attracted considerable interest, especially because of their band structure, which exhibits Dirac-like properties [9–14]. In particular, it has been shown by using *ab initio* and tight-binding (TB) methods [15] that α -graphyne features Dirac cones at the high-symmetry K and K' points of the BZ, whereas in β -graphyne they occur along the high-symmetry $\Gamma - M$ line. On the other hand, γ -graphyne is gapped. A criterion for the existence of the Dirac cones has been provided within simple TB models [16]. Furthermore, the possibility of manipula-

tion of the Dirac cones by chemical reactions has been discussed [17]. The control of the electronic properties with adatoms has been considered in Refs. [18–22], which is particularly important in light of inducing topological properties in graphyne-based materials.

Topologically nontrivial properties of the electronic band structure of a material, from a practical perspective, critically depend on the strength of the spin-orbit interaction. On the other hand, graphynes are based on carbon and, as such, are expected to feature a weak SOC, as it is the case in graphene, for instance. The effect of intrinsic SOC in these systems has been recently investigated using *ab initio* methods [23]. Furthermore, the above-mentioned possibility of controlling the electronic properties of graphynes with adatoms puts forward a way of manipulating SOC in these systems by using adatoms of heavy elements, such as Bi and Sn, for instance. Before doing so, however, a general framework for addressing SOC in graphynes has to be developed. This is precisely the aim of the present paper. The effect of SOC in β -graphyne has been previously investigated by the same authors [24]. Here, we derive a general TB theory of the spin-orbit interactions in graphynes, apply it to α - and γ -graphynes, as well as provide a comparison of the effects of the SOC in the three compounds. For completeness we also repeat some of our results on β -graphyne previously reported in Ref. [24].

We concentrate on the effect of both Rashba SOC, which can be induced by an external electric field, as well as on the intrinsic SOC. We find that the spin-orbit interactions produce different effects for α -, β -, and γ -graphyne. In α - and β -graphyne [24], the intrinsic SOC opens up a non-trivial band gap. The Rashba SOC affects α -graphyne in exactly the same way as it does for graphene: it lifts the spin degeneracy and splits each Dirac cone into four distinct Dirac cones. In β -graphyne the Rashba SOC splits each Dirac cone into two, instead of four. As the coupling is increased, this pair of cones eventually merges with another pair on the line connecting the K and K' points in the Brillouin zone. When the coupling is further increased, a new pair of Dirac

cones emerges at the line connecting the Γ and M points. Finally, in γ -graphyne the effect is the opposite as compared to β -graphyne, since now one begins with a gapped system, and if the Rashba SOC parameter exceeds a certain value, the Dirac cones emerge along the line connecting the K and K' points.

In the following, we first introduce in Sec. II the TB model for the different types of graphyne and derive the corresponding band structures without the SOC. Then, we investigate the form of the Rashba and the intrinsic SOC in Sec. III and introduce an effective model in Sec. IV. Our conclusions are drawn in Sec. V, and the details of the calculations are presented in appendices.

II. TIGHT-BINDING MODEL

The three types of graphyne can all be described in terms of a TB model that takes into account only the p_z orbitals. It was also shown that one can integrate out the contributions coming from the acetylene bonds to derive an effective model (see also Appendix A)[18,25]. By doing so, one can describe α -graphyne by the same Hamiltonian as used for graphene, but with a different value of the nearest-neighbor (NN) hopping parameter. On the other hand, β - and γ -graphyne are well described by an effective six-site model, with two hopping parameters. In the following, we discuss separately the band structure for each type of graphyne and describe the system by an effective Hamiltonian.

A. α -graphyne

Of all graphynes, α -graphyne is the simplest. One can envision α -graphyne as being obtained from graphene upon insertion of two more carbon atoms bonded by an acetylene linkage between any two carbon atoms of the honeycomb graphene lattice. As a result, the number of atoms in the unit cell grows from 2 to 8 [see Fig. 1(a)]. To describe this system in terms of a TB model, we will need two different hopping parameters: $t_{\alpha,2}$ and $t_{\alpha,3}$. Using the labeling shown in Fig. 1(a), the Hamiltonian reads as

$$H^\alpha = t_{\alpha,2} \sum_{\langle i,j \rangle} \left[A_i^\dagger (a_{1,j} + a_{2,j} + a_{3,j}) + B_i^\dagger (b_{1,j} + b_{2,j} + b_{3,j}) \right] + t_{\alpha,3} \sum_{\langle i,j \rangle} \left(a_{1,i}^\dagger b_{1,j} + a_{2,i}^\dagger b_{2,j} + a_{3,i}^\dagger b_{3,j} \right) + h.c. \quad (1)$$

By integrating out the electrons forming the acetylene bonds (see Appendix B1), we obtain an effective low-energy Hamiltonian

$$H_{\text{eff}}^\alpha = \tilde{t}_\alpha \sum_{\langle i,j \rangle} A_i^\dagger B_j + h.c., \quad (2)$$

where $\tilde{t}_\alpha = -t_{\alpha,2}^2 t_{\alpha,3} / (3t_{\alpha,2}^2 + t_{\alpha,3}^2)$. Fitting the TB parameters with a first-principles calculation [25] yields $t_{\alpha,2} = -2.85\text{eV}$ and $t_{\alpha,3} = -7.50\text{eV}$, hence $\tilde{t}_\alpha = 0.76\text{eV}$. As shown in Fig. 2(a), the band structure obtained from the low-energy approximation (red dashed lines) agrees very well with the band structure obtained from the full TB model (blue solid lines).

Since the physics around the Fermi energy in α -graphyne is described by the same Hamiltonian as graphene, it comes as no surprise that α -graphyne exhibits two Dirac cones at the K and K' points, see Figs. 2(a) and 3(a). The main difference with graphene is the reduced Fermi velocity. In graphene the Fermi velocity is given by $v_F = 3at/2\hbar \simeq 10^6$ m/s, with $t \approx -2.8\text{eV}$ the hopping amplitude [1] and a the NN distance, whereas in α -graphyne $v_F = 9a\tilde{t}_\alpha/2\hbar \simeq 7 \times 10^5$ m/s. Note that in graphene the NN distance $a = 1.42\text{\AA}$ [1], whereas in α -graphyne there are actually two different bond lengths, one for the single bond $d_s = 1.40\text{\AA}$ and one for the triple bond $d_t = 1.23\text{\AA}$ [18]. However, setting d_s and d_t equal to the bond length a in graphene yields an error smaller than 10%. As a consequence of the reduced Fermi velocity, many-body effects arising from the long-range Coulomb interaction, with effective coupling constant $\alpha = e^2/v_F$, where e is the electron charge, could be more pronounced in graphyne than in graphene.

B. β -graphyne

Among the three different types of graphyne that we consider, β -graphyne has the most complicated lattice structure. Its unit cell involves 18 atoms and consists of a hexagon, which has one carbon atom located at each vertex, and two carbon atoms connected by an acetylene bond between each two neighboring vertices [see Fig. 1(b)]. A TB description of β -graphyne requires three different hopping parameters: $t_{\beta,1}$, $t_{\beta,2}$, and $t_{\beta,3}$. Using the labeling displayed in Fig. 1(b), the TB Hamiltonian reads as

$$H^\beta = t_{\beta,1} \sum_{\langle i,j \rangle} \left(A_i^\dagger D_j + B_i^\dagger E_j + C_i^\dagger F_j \right) + t_{\beta,2} \sum_{\langle i,j \rangle} \left[A_i^\dagger (a_{1,j} + a_{2,j}) + B_i^\dagger (b_{1,j} + b_{2,j}) + C_i^\dagger (c_{1,j} + c_{2,j}) + D_i^\dagger (d_{1,j} + d_{2,j}) + E_i^\dagger (e_{1,j} + e_{2,j}) + F_i^\dagger (f_{1,j} + f_{2,j}) \right] + t_{\beta,3} \sum_{\langle i,j \rangle} \left(a_{1,i}^\dagger b_{1,j} + b_{2,i}^\dagger c_{2,j} + c_{1,i}^\dagger d_{1,j} + d_{2,i}^\dagger e_{2,j} + e_{1,i}^\dagger f_{1,j} + f_{2,i}^\dagger a_{2,j} \right) + h.c. \quad (3)$$

By performing a Fourier transformation and subsequently eliminating the high-energy orbitals (see Appendix B2), we obtain an effective six-site model. The

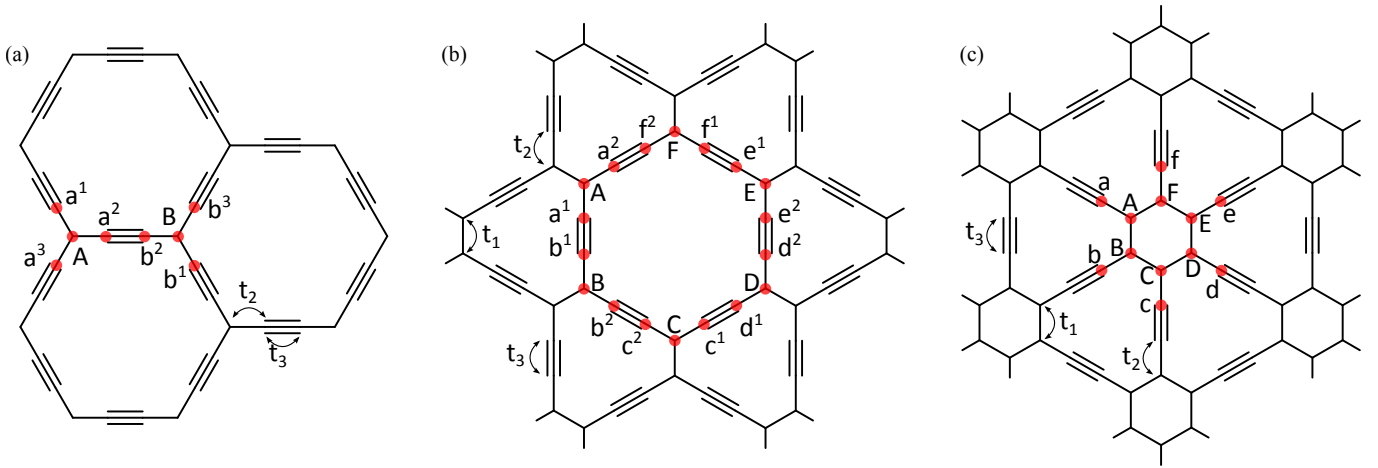


FIG. 1: (Color online) Lattice structure of α -, β - and γ -graphyne, shown in panels (a), (b), and (c), respectively. Atoms at the vertices are denoted by capital letters, whereas atoms located at the edges are denoted by lower-case letters. The hopping parameters t_i are also shown, with the subscripts 1, 2, and 3 corresponding to vertex-vertex, vertex-edge, and edge-edge hoppings, respectively.

effective low-energy Hamiltonian reads as

$$H_{\text{eff}}^{\beta} = t_{\text{int}}^{\beta} \sum_{\langle i,j \rangle} \left[A_i^{\dagger} (B_j + F_j) + C_i^{\dagger} (B_j + D_j) + E_i^{\dagger} (D_j + F_j) \right] + t_{\text{ext}}^{\beta} \sum_{\langle i,j \rangle} \left[A_i^{\dagger} D_j + C_i^{\dagger} F_j + E_i^{\dagger} B_j \right] + h.c., \quad (4)$$

where $t_{\text{int}}^{\beta} = -t_{\beta,2}^2 t_{\beta,3} / (2t_{\beta,2}^2 + t_{\beta,3}^2)$ and $t_{\text{ext}}^{\beta} = t_{\beta,1} t_{\beta,3}^2 / (2t_{\beta,2}^2 + t_{\beta,3}^2)$. In β -graphyne, it is found [25] that $t_{\beta,1} = -2.00\text{eV}$, $t_{\beta,2} = -2.70\text{eV}$, and $t_{\beta,3} = -4.30\text{eV}$, hence $t_{\text{int}}^{\beta} = 0.95\text{eV}$ and $t_{\text{ext}}^{\beta} = -1.12\text{eV}$. It turns out that the agreement between this effective model (red dashed lines) and the full TB Hamiltonian (blue solid lines) is extremely good [see Fig. 2(b)]. The dispersion relation exhibits six Dirac cones, located on the line $\Gamma - M$ [see also Fig. 3(b)]. As opposed to graphene and α -graphyne, where the cones exhibit a threefold symmetry, in β -graphyne the cones are symmetric under mirror reflection through the normal plane containing the line $\Gamma - M$ [15].

C. γ -graphyne

γ -graphyne has a somewhat simpler structure than β -graphyne, as its unit cell contains only 12 atoms [see Fig. 1(c)]. The TB description of γ -graphyne involves three hopping parameters: $t_{\gamma,1}$, $t_{\gamma,2}$, and $t_{\gamma,3}$. Using the

labeling shown in Fig. 1(c), we find that H^{γ} is given by

$$H^{\gamma} = t_{\gamma,1} \sum_{\langle i,j \rangle} \left[A_i^{\dagger} (B_j + F_j) + C_i^{\dagger} (B_j + D_j) + E_i^{\dagger} (D_j + F_j) \right] + t_{\gamma,2} \sum_{\langle i,j \rangle} \left(A_i^{\dagger} a_j + B_i^{\dagger} b_j + C_i^{\dagger} c_j + D_i^{\dagger} d_j + E_i^{\dagger} e_j + F_i^{\dagger} f_j \right) + t_{\gamma,3} \sum_{\langle i,j \rangle} \left(a_i^{\dagger} d_j + b_i^{\dagger} e_j + c_i^{\dagger} f_j \right) + h.c. \quad (5)$$

As for β -graphyne, here we also perform a Fourier transformation (see Appendix B3), and then eliminate the high-energy orbitals, to obtain the effective model

$$H_{\text{eff}}^{\gamma} = t_{\text{int}}^{\gamma} \sum_{\langle i,j \rangle} \left[A_i^{\dagger} (B_j + F_j) + C_i^{\dagger} (B_j + D_j) + E_i^{\dagger} (D_j + F_j) \right] + t_{\text{ext}}^{\gamma} \sum_{\langle i,j \rangle} \left[A_i^{\dagger} D_j + C_i^{\dagger} F_j + E_i^{\dagger} B_j \right] + h.c., \quad (6)$$

with $t_{\text{int}}^{\gamma} = t_{\gamma,1} t_{\gamma,3}^2 / (t_{\gamma,2}^2 + t_{\gamma,3}^2)$ and $t_{\text{ext}}^{\gamma} = -t_{\gamma,2}^2 t_{\gamma,3} / (t_{\gamma,2}^2 + t_{\gamma,3}^2)$. Mapping this TB model to DFT calculations [25] yields $t_{\gamma,1} = -2.75\text{eV}$, $t_{\gamma,2} = -3.11\text{eV}$, and $t_{\gamma,3} = -4.04\text{eV}$, hence $t_{\text{int}}^{\gamma} = -1.73\text{eV}$ and $t_{\text{ext}}^{\gamma} = 1.50\text{eV}$. The band structure does not exhibit any Dirac points at the Fermi energy [see Figs. 2(c) and 3(c)]. The gap at the M point is approximately equal to 0.44eV . Notice that the low-energy approximation is less accurate for γ -graphyne than for α - and β -graphyne due to the presence of a band gap.

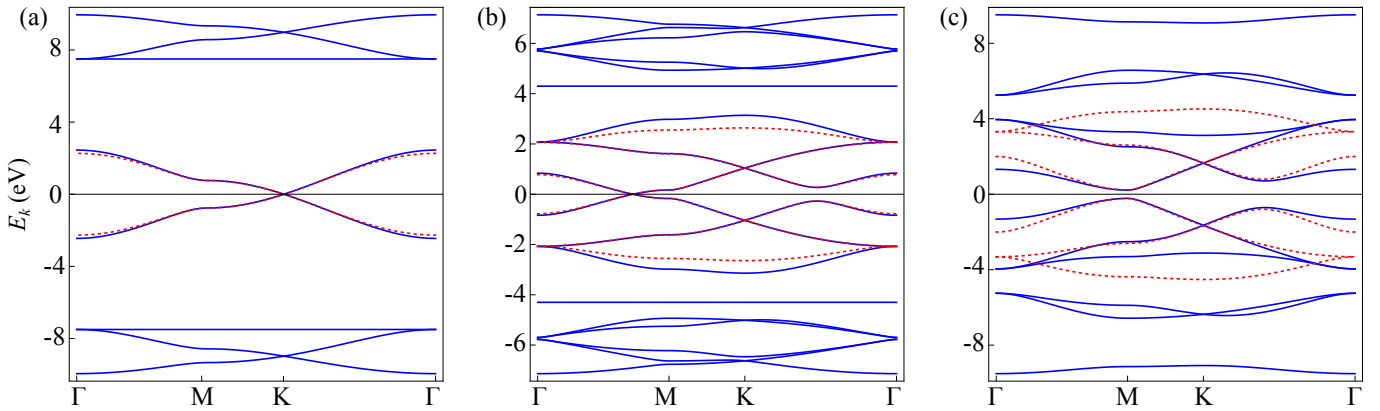


FIG. 2: (Color online) Dispersion relation for α -, β -, and γ -graphyne along high-symmetry lines, shown in (a), (b), and (c), respectively. The (blue) solid lines correspond to the dispersion relation obtained from the full TB Hamiltonian, whereas the (red) dashed lines correspond to the dispersion relation obtained from the low-energy approximation.

III. SPIN-ORBIT COUPLING

Whereas the SOC has been extensively studied in graphene, this coupling has so far been rather unexplored in graphynes. In this section, we derive the TB Hamiltonians corresponding to both Rashba and intrinsic SOC. Moreover, we show how the effective coupling parameters are related to the microscopic hopping parameters.

The intrinsic SOC originates from relativistic corrections to the Schrödinger equation. By expanding the Dirac equation up to second order in v/c , with v denoting the electron velocity, one finds that the microscopic Hamiltonian acquires an additional term

$$H_L = -\frac{\hbar}{4mc^2} \boldsymbol{\sigma} \cdot (\mathbf{p} \times \nabla V), \quad (7)$$

where $\boldsymbol{\sigma}$ is a vector of Pauli matrices, \mathbf{p} is the momentum, m is the electron mass, and V is the nuclear potential [26]. If one rewrites this expression in spherical coordinates, one obtains

$$H_L = -f(r) \boldsymbol{\sigma} \cdot \mathbf{L}, \quad (8)$$

where f is a function that goes rapidly to zero away from the origin and \mathbf{L} is the orbital angular momentum. In or-

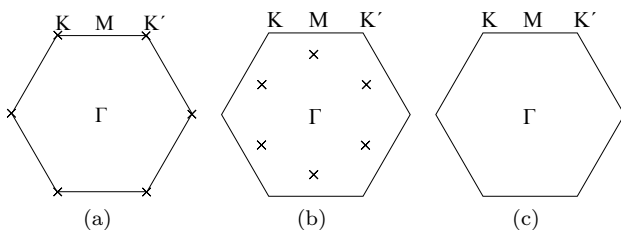


FIG. 3: Sketch of the BZ for α -, β -, and γ -graphyne, shown in panels (a), (b), and (c), respectively. The crosses correspond to Dirac cones.

der to see how this additional Hamiltonian enters the TB models, we need to reconsider the derivation presented in Sec. II. The models we considered therein only describe the band-structure due to the p_z orbitals, but the bonds in graphyne are formed by the s , p_x , and p_y orbitals, called σ orbitals due to their symmetry. When SOC is not involved, the σ and p_z orbitals decouple since the former are even and the latter are odd with respect to mirror reflection through the $x-y$ plane. The inclusion of spin changes this picture drastically. Reflection through the $x-y$ plane is represented by σ_z in spin-space and therefore spin up ($|\uparrow\rangle$) is even, whereas spin down ($|\downarrow\rangle$) is odd under this transformation. Hence, this symmetry allows now for the coupling between $p_{z,\uparrow}$, $p_{x,\downarrow}$, $p_{y,\downarrow}$, and s_{\downarrow} orbitals, which are odd under this reflection. Analogously, it follows that the orbitals $p_{z,\downarrow}$, $p_{x,\uparrow}$, $p_{y,\uparrow}$, and s_{\uparrow} , even under this symmetry operation, can be coupled. Moreover, when an external electric field is applied perpendicularly to the $x-y$ plane, the microscopic Hamiltonian includes an extra term

$$H_E = Ez, \quad (9)$$

with E the magnitude of the applied electric field. This microscopic Hamiltonian H_E couples now the s orbitals to the p_z orbitals. This occurs as a consequence of the broken mirror symmetry. It turns out that the combination of the terms H_L and H_E leads to the Rashba SOC, while H_L alone leads to the intrinsic SOC. Hence, to describe SOC in graphyne it is necessary to include both the p_z - and the σ -orbitals. On top of the SOC generated by the σ -orbitals, we also need to consider the effect of the d_{xz} and d_{yz} orbitals, as it has been shown before for graphene [27]. However, the nature of this effect is entirely different in graphynes, because even without considering spin, the p_z orbitals already couple to the d_{xz} and d_{yz} orbitals. The intrinsic SOC leads to a spin dependent on-site hoppings between the d_{xz} and d_{yz} orbitals. In the following, we discuss separately the SOC generated by the σ -orbitals and by the d -orbitals.

A. Spin-orbit coupling generated by the σ -orbitals

Since we have to include the σ -orbitals and spin, the number of orbitals in the TB models increases by a factor of 8 (2 for spin, 4 for orbitals). The corresponding Hamiltonian reads as

$$H = H_z + H_\sigma + H_{SOC}^{z,\sigma} + (H_{SOC}^{z,\sigma})^\dagger, \quad (10)$$

where H_z describes the p_z orbitals, H_σ describes the σ orbitals (see Appendix C), and $H_{SOC}^{z,\sigma}$ accounts for the hopping from p_z orbitals to σ -orbitals due to the SOC. The latter can be decomposed as

$$H_{SOC}^{z,\sigma} = H_L^{z,\sigma} + H_E^{z,\sigma}, \quad (11)$$

with the orbital angular momentum and electric field terms given by

$$H_L^{z,\sigma} = \xi_{p1} \sum_i' p_{z,i}^\dagger (-i\sigma_y p_{x,i} + i\sigma_x p_{y,i}) \quad (12)$$

$$+ \xi_{p2} \sum_i'' p_{z,i}^\dagger (-i\sigma_y p_{x,i} + i\sigma_x p_{y,i}),$$

$$H_E^{z,\sigma} = \xi_{sp1} \sum_i' p_{z,i}^\dagger s_i + \xi_{sp2} \sum_i'' p_{z,i}^\dagger s_i, \quad (13)$$

where $p_{z,i}^\dagger$ creates an electron in a p_z orbital at position i , and analogous notation is used for the p_x , p_y , and s orbitals. The exact value of the on-site coupling parameters ξ_{p1} , ξ_{p2} , ξ_{sp1} , and ξ_{sp2} may be obtained by fitting the band structure to first-principles calculations. Note that ξ_{sp1} and ξ_{sp2} are both linear in E . Furthermore, the prime (double prime) in the summation indicates that the sum is taken over atoms located at the edges (vertices). These terms result from considering the matrix elements $\boldsymbol{\sigma} \cdot \mathbf{L}$ and Ez (see also Table I). Let us consider the matrix element $\langle p_z | \boldsymbol{\sigma} \cdot \mathbf{L} | p_x \rangle$, as an example. As a first step, we rewrite L_x and L_y in terms of raising and lowering operators,

$$\begin{aligned} L_x &= \frac{1}{2}(L_+ + L_-), \\ L_y &= -\frac{i}{2}(L_+ - L_-). \end{aligned} \quad (14)$$

Next, one rewrites the atomic orbitals $|p_x\rangle$, $|p_y\rangle$, and $|p_z\rangle$ in terms of the simultaneous eigenstates of the operators H , L^2 and L_z , $|n, l, m\rangle$. Since all the orbitals we consider are in the second shell, $n = 2$, we simply write $|2, l, m\rangle \equiv |l, m\rangle$. Then, we have

$$\begin{aligned} |p_x\rangle &= \frac{1}{\sqrt{2}}(-|1, 1\rangle + |1, -1\rangle), \\ |p_y\rangle &= \frac{i}{\sqrt{2}}(|1, 1\rangle + |1, -1\rangle), \\ |p_z\rangle &= |1, 0\rangle, \end{aligned} \quad (15)$$

yielding

$$\begin{aligned} L_x |p_x\rangle &= \frac{1}{2} \frac{1}{\sqrt{2}}(L_+ + L_-)(-|1, 1\rangle + |1, -1\rangle) \\ &= \frac{1}{2}(-|1, 0\rangle + |1, 0\rangle) = 0. \end{aligned} \quad (16)$$

Similarly, we find

$$L_y |p_x\rangle = -i|p_z\rangle. \quad (17)$$

As a result, we obtain $\langle p_z | \boldsymbol{\sigma} \cdot \mathbf{L} | p_x \rangle = \langle p_z | -i\sigma_y | p_x \rangle = -i\sigma_y$, where we also used $\langle p_z | L_z | p_x \rangle = 0$.

Since the p_z -orbitals correspond to the low-energy states, we can use the approximation scheme outlined in the App. A, which yields

$$\begin{aligned} H_{z,v+e}^{\text{eff}} &= S^{-1/2}(H_z - H_{SOC}^{z,\sigma} H_\sigma^{-1} (H_{SOC}^{z,\sigma})^\dagger) S^{-1/2}, \\ &= S^{-1/2} H_z S^{-1/2} \\ &\quad - S^{-1/2} H_{SOC}^{z,\sigma} H_\sigma^{-1} (H_{SOC}^{z,\sigma})^\dagger S^{-1/2}. \end{aligned} \quad (18)$$

In the second line, we have split the Hamiltonian in two parts. The first term on the right-hand side (RHS) can neither lead to the opening of a gap, nor can it shift the position of the Dirac cones. This follows from the relation $\det[S^{-1/2} H_z S^{-1/2}] = \det H_z / \det S$. Hence, as for the first term, we may simply set $S = \mathbb{I}$. With respect to the second term, we use

$$S^{-1/2} = \mathbb{I} - \frac{1}{2} H_{SOC}^{z,\sigma} H_\sigma^{-1} (H_{SOC}^{z,\sigma})^\dagger + \dots \quad (19)$$

This shows that if we use \mathbb{I} , we neglect contributions proportional to ξ^4 in the second term, with $\xi \in \{\xi_{sp1}, \xi_{sp2}, \xi_{p1}, \xi_{p2}\}$. This is allowed, since all ξ 's are very small compared to the other hopping parameters. As a result, we approximate the effective Hamiltonian by

$$H_{z,v+e}^{\text{eff}} = H_z - H_{SOC}^{z,\sigma} H_\sigma^{-1} (H_{SOC}^{z,\sigma})^\dagger. \quad (20)$$

Since in this approximation the Hamiltonian is given in momentum-space, we need to perform an inverse Fourier transformation to obtain a real-space TB Hamiltonian. Using that the hoppings which form the bonds are the largest energies in the system, we can simplify H_σ^{-1} . First of all, we use sp , sp^2 , and p hybrid orbitals, shown in Figs. 4(a), (b), and (c). In this model, we only take into account the on-site energies ε_i , on-site hoppings V_5, \dots, V_9 , as well as the NN hoppings V_1, \dots, V_4 which form a bond, yielding

$$H_\sigma = H_{\sigma,\text{onsite}} + H_{\sigma,\text{NN}}. \quad (21)$$

$\boldsymbol{\sigma} \cdot \mathbf{L} \parallel$	$ p_x\rangle$	$ p_y\rangle$	$ s\rangle$
p_z	0	$-i\sigma_y$	$i\sigma_x$

TABLE I: Matrix elements for $\boldsymbol{\sigma} \cdot \mathbf{L}$. Note that the Pauli matrices act in spin space.

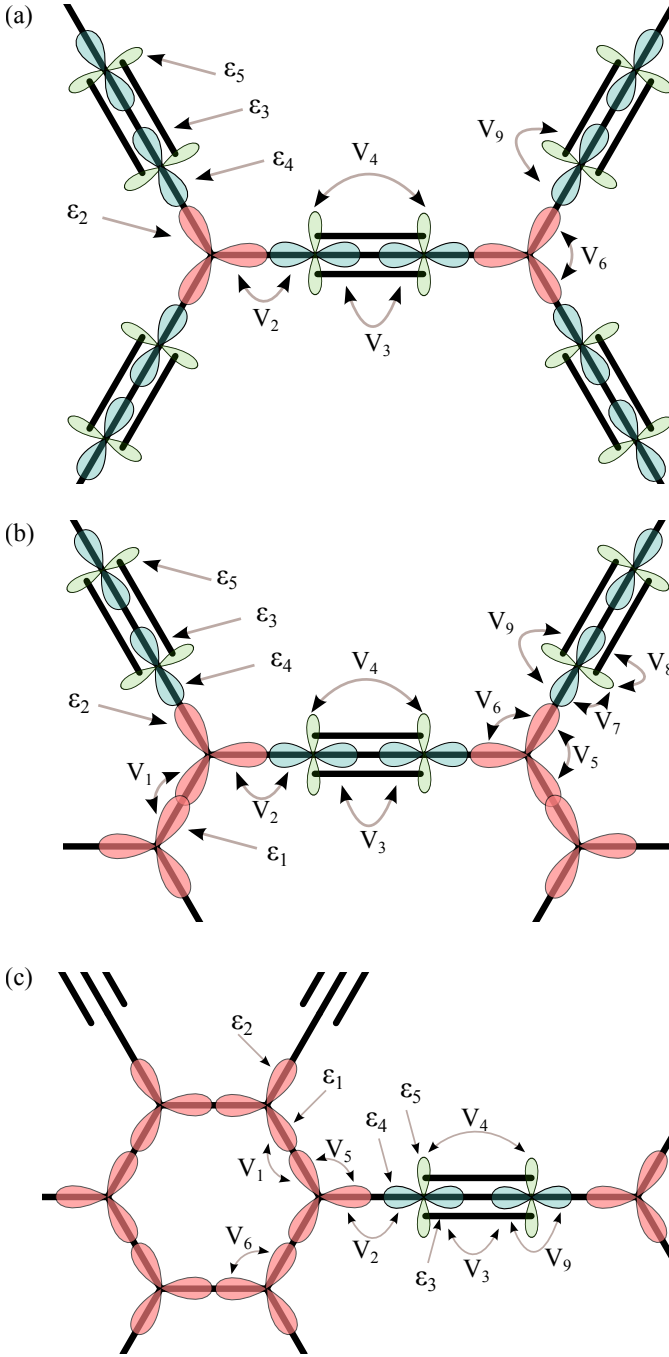


FIG. 4: (Color online) Parameters used for the σ -TB models for α , β , and γ -graphyne, shown in panels (a), (b), and (c). The hopping parameters V_1, \dots, V_4 correspond to NN hoppings, whereas V_5, \dots, V_9 correspond to on-site hoppings, and $\varepsilon_1, \dots, \varepsilon_5$ denote the on-site energies. Other hopping parameters have been set to zero.

If the on-site energies and hopping parameters of the hybrid orbitals are smaller than the NN-hopping parameters of the bonds, we may approximate the inverse matrix by

$$H_{\sigma}^{-1} \approx H_{\sigma, \text{NN}}^{-1} - H_{\sigma, \text{NN}}^{-1} H_{\sigma, \text{onsite}} H_{\sigma, \text{NN}}^{-1}. \quad (22)$$

This approximation is justified by the fact that the hybrid orbitals are mainly composed of p orbitals that have very small on-site energies. In this simple TB model, we find that

$$\left(H_{\sigma, \text{NN}}^{-1} \right)_{ij} = \begin{cases} 1 / (H_{\sigma, \text{NN}})_{ij}^* & \text{if } (H_{\sigma, \text{NN}})_{ij} \neq 0 \\ 0 & \text{if } (H_{\sigma, \text{NN}})_{ij} = 0. \end{cases} \quad (23)$$

This expression can easily be transformed to real space. The effective SOC Hamiltonian is then given by the second term on the RHS of Eq. (20) combined with Eq. (22),

$$H_{\text{SOC,eff}} = H_{\text{SOC}}^{z, \sigma} \left(H_{\sigma, \text{NN}}^{-1} - H_{\sigma, \text{NN}}^{-1} H_{\sigma, \text{onsite}} H_{\sigma, \text{NN}}^{-1} \right) (H_{\text{SOC}}^{z, \sigma})^{\dagger}. \quad (24)$$

Using the Hamiltonians $H_{\text{SOC}}^{z, \sigma}$, $H_{\sigma, \text{NN}}$, and $H_{\sigma, \text{onsite}}$ for α -, β -, and γ -graphyne, we obtain the SOC in real space

$$H_{\text{SOC,eff}}^{\sigma} = H_{\text{R}}^{\sigma} + H_{\text{I}}^{\sigma} + H_{\text{rest}}^{\sigma}, \quad (25)$$

where

$$H_{\text{R}}^{\sigma} = i \sum_{\langle i, j \rangle} \lambda_{\text{R}, ij}^{\sigma} p_{z, i}^{\dagger} \left(\boldsymbol{\sigma} \times \hat{\mathbf{d}}_{ij} \right) \cdot \hat{\mathbf{z}} p_{z, j}, \quad (26)$$

$$H_{\text{I}}^{\sigma} = i \sum_{\langle\langle i, j \rangle\rangle} \lambda_{\text{I}, ij}^{\sigma} v_{ij} p_{z, i}^{\dagger} \sigma_z p_{z, j}, \quad (27)$$

and H_{rest} describes the next-nearest neighbor (NNN) corrections to the Rashba SOC (which can be neglected), together with some very small spin-independent and thus negligible NN and NNN hoppings and on-site energies. In both expressions, we have included bond-dependent coupling constants $\lambda_{\text{R}, ij}^{\sigma}$ and $\lambda_{\text{I}, ij}^{\sigma}$, $\hat{\mathbf{d}}_{ij}$ is the unit vector pointing from site i to j , and $v_{ij} = +(-)$ if the hopping is (anti)-clockwise, and zero if it is along the acetylene bond. In total, we need six different coupling parameters to completely describe SOC in graphyne: three for Rashba ($\lambda_{\text{R}, i}^{\sigma}$) and three for the intrinsic SOC ($\lambda_{\text{I}, i}^{\sigma}$), with $i = 1, 2, 3$ corresponding to vertex-vertex, vertex-edge, and edge-edge hoppings, respectively. In Table II we give the expressions for these coupling parameters in terms of the hopping parameters for the σ -orbitals, as obtained from Eqs. (26) and (27).

It turns out that for the three types of graphyne that we consider, we obtain Hamiltonians of the same form as in graphene, simply with adjusted coupling parameters. However, in β -graphyne there is an additional contribution to the intrinsic SOC Hamiltonian. In α - and γ -graphyne, each hopping along a straight path yields no contribution to the intrinsic SOC Hamiltonian, which is a consequence of the mirror symmetry through the acetylene bond in these systems. This symmetry is weakly broken in β -graphyne. As a result of this weak symmetry breaking, we obtain a very small additional contribution to the intrinsic SOC Hamiltonian,

$$H_{\beta, 4}^{\sigma} = i \lambda_{\text{I}, 4}^{\sigma} \sum_{\langle\langle i, j \rangle\rangle} w_{ij} p_{z, i}^{\dagger} \sigma_z p_{z, j}, \quad (28)$$

where $w_{ij} = +(-)$ if the hopping is along the acetylene bond going (anti-)clockwise with respect to the center of the unit-cell, and $\lambda_{I,4}^\sigma = \sqrt{2}\xi_{p1}\xi_{p2}V_7/(\sqrt{3}V_2V_4)$. Since V_7 is non-zero only in β -graphyne, this contribution is absent in α - and γ -graphyne. Furthermore, we would like to point out that in the TB models that we used, we have neglected subdominant NN hoppings. However, the inclusion of these can lead to an NN intrinsic SOC term in the Hamiltonian. In β -graphyne, this is generated by the NN hopping from the sp^2 orbitals to the p orbitals, whereas in γ -graphyne this is caused by the hopping between sp^2 orbitals which point in different directions. These contributions can easily be explained from the broken mirror symmetry through the acetylene bond in β -graphyne, and through the σ -bond forming the hexagon in γ -graphyne. Since these symmetries are only weakly broken, their effect will be very small.

In Ref. [23], the effect of intrinsic SOC on the dispersion relation in graphyne was calculated from first principles. The predicted gap of 0.014 meV in α -graphyne is rather large as compared to graphene, and may be attributed to the inhomogeneity in the charge distribution around the acetylene bond. By fitting the gap obtained within the TB model to the one derived from first-principles calculations, we find that for α -graphyne $\lambda_{I,3}^\sigma \approx 0.041\text{meV}$. In α -graphyne $V_6 = \epsilon_s/3 \approx 2.67\text{eV}$, and a rough estimate yields $V_2 \approx 5 - 10\text{eV}$. This leads to an approximate lower bound for $\xi_{p1} \approx 12.6\text{meV}$, whereas in graphene $\xi_p \approx 2.8\text{meV}$. In addition, around the vertices the charge is rather homogeneously distributed, and thus we expect that the coupling ξ_{p2} is roughly of the same size as in graphene, i.e. $\xi_{p2} \approx 2.8\text{meV}$.

Inspection of Table II clearly shows that the parameters corresponding to the Rashba coupling are proportional to $\xi_{sp}\xi_p/V_i$, where V_i is one of the NN hopping parameters. This is expected, since the Rashba terms arise from

$$H_E^{z,\sigma} H_{\sigma,\text{NN}}^{-1} (H_L^{z,\sigma})^\dagger + h.c., \quad (29)$$

where the matrix $H_E^{z,\sigma}$ contributes a factor ξ_{sp} , H_{NN} yields a factor V_i , and $H_L^{z,\sigma}$ a factor ξ_p . Note that V_4 does not appear in Table II; this can be understood from the matrix structure of Eq. (29). Terms from right to left in this expression correspond to (i) the on-site hopping from a p_z orbital to a hybrid orbital, (ii) subsequent hopping between two NN hybrid orbitals, and (iii) the on-site hopping from an sp or sp^2 hybrid orbital to a p_z orbital due to the electric field. Since V_4 is responsible for the hopping between two NN p orbitals, it does not contribute to this process. Notice also that the parameters $\varepsilon_1, \dots, \varepsilon_5$ and V_5, \dots, V_9 do not appear here because they correspond to on-site energies and hoppings, respectively.

The intrinsic SOC arises from

$$H_L^{z,\sigma} H_{\sigma,\text{NN}}^{-1} H_{\sigma,\text{onsite}} H_{\sigma,\text{NN}}^{-1} (H_L^{z,\sigma})^\dagger + h.c.; \quad (30)$$

hence, the coupling parameters are all of the form $\xi_p^2 AB^{-2}$, where $A \in \{V_5, \dots, V_9, \varepsilon_1, \dots, \varepsilon_5\}$ comes from $H_{\sigma,\text{onsite}}$ and $B \in \{V_1, \dots, V_4\}$ comes from $H_{\sigma,\text{NN}}$. However, Table II clearly shows that actually none of these parameters are proportional to an onsite energy ε_i . The reason for this can be understood as follows. Reading Eq. (30) from right to left, we find that (i) the first matrix leads to the hopping from a p_z orbital to one of the hybrid orbitals due to the SOC, (ii) then $H_{\sigma,\text{NN}}^{-1}$ leads to the hopping to a NN hybrid orbital, (iii,a) the term $H_{\sigma,\text{onsite}}$ can lead to the onsite hopping to another hybrid orbital; this contributes a factor V_j with $j = 5, \dots, 9$, (iii,b) or it can simply stay on the same orbital which would contribute a factor ε_i . Therefore, only this last scenario would yield a contribution proportional to ε_i . However, this scenario then subsequently leads to the hopping to the hybrid orbital where one started; therefore there are no terms proportional to ε_i . The parameter V_8 is also absent in Table II. This can be understood by analyzing the hopping process proportional to V_8 : starting from the p_z orbital a^1 (see Appendix C 2, Fig. 14 therein, and Fig. 4), we then find the following:

1. $(H_L^{z,\sigma})^\dagger$ contributes a factor proportional to σ_y , and leads to the hopping to state a_1^1 .
2. $H_{\sigma,\text{NN}}^{-1}$ contributes a factor V_3^{-1} , and leads to the hopping to state b_1^1 .
3. $H_{\sigma,\text{onsite}}$ contributes a factor V_8 , and leads to the hopping to state b_3^1 .
4. $H_{\sigma,\text{NN}}^{-1}$ contributes a factor V_3^{-1} , and leads to the hopping to state a_1^1 .
5. $(H_L^{z,\sigma})^\dagger$ contributes a factor proportional to σ_y , and leads to the hopping to the p_z -orbital a^1 .

Hence, the term proportional to V_8 does not lead to a NNN hopping process, but gives rise to an onsite energy, which can be neglected. Concerning the absence of V_9 and V_3 in Table II for the intrinsic SOC parameters, we would like to point out that these terms do actually lead to a NNN hopping in Eq. (30) that is, however, spin-independent. This can be seen from the fact that from right to left again, for this process the hybrid orbital to which the p_z orbital hops points in the same direction as the hybrid orbital from which it hops to the NNN p_z orbital. To illustrate this process, we consider the hopping from A to b^1 via V_9 and V_3 (see Fig. 14 and Fig. 4):

1. $(H_L^{z,\sigma})^\dagger$ contributes a factor proportional to σ_y , and leads to the hopping to state A_2 .
2. $H_{\sigma,\text{NN}}^{-1}$ contributes a factor $1/V_2$, and leads to the hopping to state a_2^1 .

σ	$\alpha, \beta,$ and γ
$\lambda_{R,1}^\sigma$	$2\sqrt{2}\xi_{2sp}\xi_{2p}/(3V_1)$
$\lambda_{R,2}^\sigma$	$(\sqrt{2}\xi_{sp1}\xi_{p2} + \xi_{sp2}\xi_{p1})/(\sqrt{6}V_2)$
$\lambda_{R,3}^\sigma$	$\xi_{1sp}\xi_{1p}/V_3$
$\lambda_{I,1}^\sigma$	$V_6\xi_{p,2}^2/(\sqrt{3}V_1^2)$
$\lambda_{I,2}^\sigma$	$V_5\xi_{p,2}\xi_{p,1}/(2V_1V_2)$
$\lambda_{I,3}^\sigma$	$\sqrt{3}V_6\xi_{p1}^2/(4V_2^2)$
$\lambda_{I,4}^\sigma$	$\sqrt{2}\xi_{p1}\xi_{p2}V_7/(\sqrt{3}V_2V_4)$

TABLE II: SOC parameters for the three types of graphyne arising from the σ -orbitals.

d	$\alpha, \beta,$ and γ
$\lambda_{I,1}^d$	$\sqrt{3}V_{dp1}^2\xi_d/2\epsilon_d^2$
$\lambda_{I,2}^d$	$\sqrt{3}V_{dp1}V_{dp2}\xi_d/2\epsilon_d^2$
$\lambda_{I,3}^d$	$\sqrt{3}V_{dp2}^2\xi_d/2\epsilon_d^2$

TABLE III: SOC parameters for the three types of graphyne arising from the d -orbitals.

3. $H_{\sigma,\text{onsite}}$ contributes a factor V_9 , and leads to the hopping to state a_1^1 .
4. $H_{\sigma,\text{NN}}^{-1}$ contributes a factor $1/V_3$, and leads to the hopping to state b_1^1 .
5. $(H_L^{z,\sigma})^\dagger$ contributes a factor proportional to σ_y , and leads to the hopping to state b^1 .

Since the initial and final hoppings are both proportional to σ_y , we find that the combination is proportional to $\sigma_y \cdot \sigma_y = \mathbb{I}$; hence, it does not lead to a spin-dependent hopping. Note that the parameters V_4 and V_7 appear in the expression for $\lambda_{I,4}^\sigma$ in Eq. (28).

B. Spin-orbit coupling generated by the d -orbitals.

The preceding discussion showed that the coupling parameters for the intrinsic SOC are of second order in ξ_{p1} and (or) ξ_{p2} . In Ref. [27], it was shown that the gap opening in graphyne is actually due to intrinsic SOC hosted by the d_{xz} and d_{yz} orbitals. The reason is that the intrinsic SOC due to the d orbitals is of first order in the intrinsic SOC parameter for the d -orbitals, ξ_d . To include the contributions stemming from the d -orbitals, we write the TB Hamiltonian with the hopping between the p_z , d_{xz} , and d_{yz} orbitals included, and the intrinsic SOC among the d -orbitals

$$H = H_z + H_{zd} + H_{zd}^\dagger + H_d + H_L^d. \quad (31)$$

Here, H_z describes the hopping between the p_z orbitals, H_{zd} describes the hopping from the d orbitals to the p_z orbitals, H_d is the TB Hamiltonian describing the d_{xz} and d_{yz} orbitals, and H_L^d describes the intrinsic SOC between the d_{xz} and d_{yz} orbitals. The latter term is given

by

$$H_L^d = i\xi_{d1} \sum_i' d_{yz,i}^\dagger \sigma_z d_{xz,i} + i\xi_{d2} \sum_i'' d_{yz,i}^\dagger \sigma_z d_{xz,i} + h.c. \quad (32)$$

The Hamiltonian H_{zd} is given by

$$H_{zd} = \sum_{\langle i,j \rangle} V_{dp,ij} p_{z,i}^\dagger (\hat{\mathbf{d}}_{ij}^x d_{xz,j} + \hat{\mathbf{d}}_{ij}^y d_{yz,j}), \quad (33)$$

where $\hat{\mathbf{d}}_{ij}^\mu$ is the μ -component of the vector $\hat{\mathbf{d}}_{ij}$, defined below Eq. (27) and $V_{dp,ij} = V_{dp,k}$ with $k = 1, 2, 3$ depending whether $\hat{\mathbf{d}}_{ij}$ points from vertex to vertex, vertex to edge or edge to edge, respectively. Again, we use the approximation scheme from Appendix A that leads to the following effective Hamiltonian:

$$H_{z,v+e}^{\text{eff}} = S^{-1/2} [H_z - H_{zd} (H_L^d + H_d)^{-1} H_{zd}^\dagger] S^{-1/2}. \quad (34)$$

Following the same reasoning as before, we simply set $S = \mathbb{I}$. Since ξ_{d1} and ξ_{d2} are very small, we may approximate $(H_L^d + H_d)^{-1} \approx H_d^{-1} - H_d^{-1} H_L^d H_d^{-1}$. Notice that this explains why the intrinsic SOC generated by the d -orbitals is first order in ξ_d . As a result, the effective intrinsic SOC Hamiltonian due to the d -orbitals is given by

$$H_{\text{SOC,eff}} = H_{zd} H_d^{-1} H_L^d H_d^{-1} H_{zd}^\dagger. \quad (35)$$

Because of the large on-site energies of the d orbitals ϵ_d , we may approximate $H_d^{-1} \approx \epsilon_d^{-1} \mathbb{I}$. Therefore, Eq. (35) reduces to

$$H_{\text{SOC,eff}} = H_{zd} H_L^d H_{zd}^\dagger / \epsilon_d^2. \quad (36)$$

Using the Hamiltonians H_L^d and H_{zd} , we finally obtain the intrinsic SOC Hamiltonian due to the d -orbitals,

$$H_I^d = i \sum_{\langle\langle i,j \rangle\rangle} \lambda_{I,ij}^d v_{ij} p_{z,i}^\dagger \sigma_z p_{z,j}, \quad (37)$$

where $v_{ij} = (+)-$ if the hopping is (anti)-clockwise. As for the σ -orbitals, we will need three different coupling parameters ($\lambda_{I,i}^d$) to completely describe intrinsic SOC; the labeling used is the same as for the σ -orbitals. The coupling parameters are given in Table III. Note that the expressions for the SOC parameters due to the d -orbitals and due to the σ -orbitals have the same sign. Therefore, the intrinsic SOC is governed by the parameters $\lambda_{I,j}^\sigma = \lambda_{I,j}^\sigma + \lambda_{I,j}^d$. As a result, the inclusion of d -orbitals increases the effect of SOC in graphynes.

In Ref. [27], it was shown that the effect of d -orbitals on the Rashba SOC is negligible. We expect that this remains true in graphynes, and for this reason we have not considered the effect of d -orbitals on the Rashba SOC.

SOC	$\alpha, \beta,$ and γ
$\tilde{\lambda}_I^\alpha$	$\lambda_{I,3}t_2^2/(t_3^2 + 3t_2^2)$
$\lambda_{\text{ext},I}^\beta$	$-\lambda_{I,2}t_2t_3/(t_3^2 + 2t_2^2)$
$\lambda_{\text{ext},I}^\gamma$	$-\lambda_{I,2}t_3t_2/(t_2^2 + t_3^2)$
$\lambda_{\text{int},I}^\beta$	$\lambda_{I,3}t_2^2/(t_3^2 + 2t_2^2)$
$\lambda_{\text{int},I}^\gamma$	$\lambda_{I,1}t_3^2/(t_2^2 + t_3^2)$
$\tilde{\lambda}_R^\alpha$	$2\lambda_{R,2}t_2t_3/(t_3^2 + 3t_2^2) + \lambda_{R,3}t_2^2/(t_3^2 + 3t_2^2)$
$\lambda_{\text{ext},R}^\beta$	$\lambda_{R,1}t_3^2/(t_3^2 + 2t_2^2)$
$\lambda_{\text{ext},R}^\gamma$	$2\lambda_{R,2}t_2t_3/(t_3^2 + t_2^2) + \lambda_{R,2}t_2^2/(t_3^2 + t_2^2)$
$\lambda_{\text{int},R}^\beta$	$-2\lambda_{R,2}t_2t_3/(t_3^2 + 2t_2^2) - \lambda_{R,3}t_2^2/(t_3^2 + 2t_2^2)$
$\lambda_{\text{int},R}^\gamma$	$\lambda_{R,1}t_3^2/(t_2^2 + t_3^2)$

TABLE IV: SOC parameters for the effective TB models.

C. Spin-orbit Hamiltonians in the two-site and six-site model

The SOC Hamiltonians that we obtained are all given in terms of the full TB Hamiltonian. The next step is to integrate out the high-energy orbitals to obtain SOC Hamiltonians that can be used in the effective models introduced in Sec. II. In general, the effective Hamiltonian reads as

$$H_{z,v}^{\text{eff}} = S^{-1/2} (H_{vv} - H_{ve}H_{ee}^{-1}H_{ve}^\dagger) S^{-1/2}, \quad (38)$$

where H_{vv} (H_{ee}) describe the orbitals at the vertices (edges), and H_{ve} mixes them. In order to incorporate SOC in this description, we write each matrix as the sum of a spin-independent part, denoted by a tilde, and a part describing the SOC, denoted by the subscript SOC. Because the SOC parameters are very small compared to the other hopping energies, we may expand Eq. (38) up to first order in them. One then readily obtains

$$\begin{aligned} S^{-1/2} &= (\tilde{S} + S_{SOC})^{-1/2}, \\ &\approx \tilde{S}^{-1/2} - \frac{1}{2}\tilde{S}^{-3/2}S_{SOC}, \end{aligned} \quad (39)$$

where

$$\begin{aligned} S_{SOC} &= H_{ve,SOC}\tilde{H}_{ee}^{-2}\tilde{H}_{ve}^\dagger \\ &\quad - \tilde{H}_{ve}\tilde{H}_{ee}^{-2}H_{ee,SOC}\tilde{H}_{ee}^{-1}\tilde{H}_{ve}^\dagger + h.c. \end{aligned} \quad (40)$$

However, if we simply set $S = \tilde{S}$ we do not miss any gap openings or shifts in the positions of the Dirac cones. Hence, we approximate Eq. (38) by

$$H_{z,v}^{\text{eff}} \approx \tilde{S}^{-1/2} (H_{vv} - H_{ve}H_{ee}^{-1}H_{ve}^\dagger) \tilde{S}^{-1/2}. \quad (41)$$

As a result, we find

$$H_{z,v}^{\text{eff}} \approx \tilde{H}_{z,v}^{\text{eff}} + H_{SOC}, \quad (42)$$

where $H_{SOC} = H_{1,SOC} + H_{2,SOC} + H_{3,SOC}$, with

$$H_{1,SOC} = \tilde{S}^{-1/2}H_{vv,SOC}\tilde{S}^{-1/2}, \quad (43)$$

$$H_{2,SOC} = -\tilde{S}^{-1/2}H_{ve,SOC}\tilde{H}_{ee}\tilde{H}_{ve}^\dagger\tilde{S}^{-1/2} + h.c., \quad (44)$$

$$H_{3,SOC} = \tilde{S}^{-1/2}\tilde{H}_{ve}\tilde{H}_{ee}^{-1}H_{ee,SOC}\tilde{H}_{ee}^{-1}\tilde{H}_{ve}^\dagger. \quad (45)$$

By performing these calculations for α -graphyne, we obtain

$$H_{R,\alpha} = i\lambda_R \sum_{\langle i,j \rangle} p_{z,i}^\dagger (\boldsymbol{\sigma} \times \hat{\mathbf{d}}_{ij}) \cdot \hat{\mathbf{z}}p_{z,j}, \quad (46)$$

$$H_{I,\alpha} = i\lambda_I \sum_{\langle\langle i,j \rangle\rangle} v_{ij}p_{z,i}^\dagger \sigma_z p_{z,j}, \quad (47)$$

which are the standard SOC Hamiltonians, as used for graphene. The results for β - and γ -graphyne are slightly different than for graphene, since now we have to distinguish between the inter and intra-unit cell SOC. We refer to the inter-unit cell SOC as external SOC, and to the intra unit cell SOC as internal SOC. The form of the SOC Hamiltonians is however unchanged as compared to graphene,

$$\begin{aligned} H_{R,\beta/\gamma} &= i\lambda_{\text{int},R} \sum_{\langle i,j \rangle} p_{z,i}^\dagger (\boldsymbol{\sigma} \times \hat{\mathbf{d}}_{ij}) \cdot \hat{\mathbf{z}}p_{z,j} \\ &\quad + i\lambda_{\text{ext},R} \sum_{\langle i,j \rangle} p_{z,i}^\dagger (\boldsymbol{\sigma} \times \hat{\mathbf{d}}_{ij}) \cdot \hat{\mathbf{z}}p_{z,j}, \end{aligned} \quad (48)$$

$$H_{I,\beta/\gamma} = i\lambda_{\text{int},I} \sum_{\langle\langle i,j \rangle\rangle} v_{ij}p_{z,i}^\dagger \sigma_z p_{z,j} \quad (49)$$

$$+ i\lambda_{\text{ext},I} \sum_{\langle\langle i,j \rangle\rangle} v_{ij}p_{z,i}^\dagger \sigma_z p_{z,j}. \quad (50)$$

Here, the single (double) dot indicates that the sum is taken over sites within the same (belonging to different) unit cells. In Table IV we have listed the effective SOC hopping parameters.

IV. INTERNAL AND EXTERNAL SPIN-ORBIT COUPLINGS

As shown in Sec. II, both β - and γ -graphyne can be described in terms of the same six-site model, and Eqs. (4)

and (6) can be rewritten in a short-hand notation as

$$H_0 = t_{\text{int}} \sum_{\langle i,j \rangle} p_{z,i}^\dagger p_{z,j} + t_{\text{ext}} \sum_{\langle i,j \rangle} p_{z,i}^\dagger p_{z,j}. \quad (51)$$

The band structure obtained from this Hamiltonian exhibits six Dirac cones at the line connecting the Γ and M points if the condition $-2 < t_{\text{ext}}/t_{\text{int}} < -1$ is satisfied. This is realized for β - but not for γ -graphyne [see Figs. 3(b) and 3(c)]. We show in the following that the intrinsic SOC can open a non-trivial gap in β -graphyne, whereas the Rashba SOC can be used to open or close a trivial gap in β - and γ -graphyne. In Eqs. (48) and (49), we have made a distinction between external and internal SOC. To obtain a better understanding of the effect of both terms, we discuss them separately in the following.

A. Internal Rashba spin-orbit coupling

The internal Rashba SOC leads to very interesting phases characterized by the presence of Dirac cones at different points in the BZ. First, we discuss the regime that applies to β -graphyne, after which we consider the regime that describes γ -graphyne. At the end we also comment on the other regimes. Part of the phase diagram is shown in Fig. 5. The red dashed line therein corresponds to β -graphyne, whereas the blue solid line corresponds to γ -graphyne.

For the regime $-1.19 < t_{\text{ext}}/t_{\text{int}} < -1$ that applies to β -graphyne, the system goes through three different phases. Initially, the internal Rashba SOC splits each Dirac cone into a pair of Dirac cones located at a line perpendicular to the line connecting the Γ - M points (see region I in Fig. 5). Upon increasing the coupling, these pairs move towards the boundary of the BZ, where they eventually annihilate with another pair at the line connecting the K and K' points. As a result, the system becomes gapped (see region II in Fig. 5). If the internal Rashba SOC is even further increased, the system undergoes another phase transition, with six new pairs of Dirac cones emerging along the lines connecting the Γ and M points (see region III in Fig. 5).

Next, we discuss the regime $-1 < t_{\text{ext}}/t_{\text{int}} < -0.8$ that describes γ -graphyne. The system is initially gapped (see also region II in Fig. 5). However, when the internal Rashba SOC is sufficiently large, six pairs of Dirac cones appear along the lines connecting the Γ - M points (see region III in Fig. 5).

Having studied the regimes that apply to β - and γ -graphyne, we now consider the regime for which $-1.26 < t_{\text{ext}}/t_{\text{int}} < -1.19$. As for β -graphyne, initially the internal Rashba SOC splits each Dirac cone into a pair of Dirac cones located along a line perpendicular to Γ - M (see region I in Fig. 5). When the internal Rashba SOC

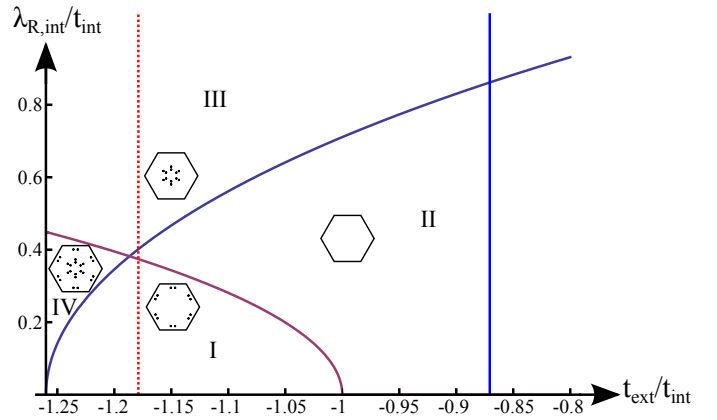


FIG. 5: (Color online) Phase diagram for the effective Hamiltonian (51) with internal Rashba SOC. In region I the system exhibits 12 Dirac cones, region II corresponds to the gapped phase, region III corresponds to the system where only pairs of Dirac cones along the line Γ - M are present, and region IV corresponds to a system where there are six pairs of cones along the line Γ - M and six pairs on lines perpendicular to Γ - M .

is even further increased, six additional pairs of Dirac cones emerge along the line connecting Γ - M (see region IV in Fig. 5). Eventually, when the coupling is even further increased, the six pairs of Dirac cones located at lines perpendicular to the Γ - M points annihilate at the boundary of the BZ (see region III in Fig. 5). Finally, when $-2 < t_{\text{ext}}/t_{\text{int}} < -1.26$, another curious phenomenon occurs (not shown in Fig. 5). First, each Dirac cone splits into a pair along the line connecting the Γ and M points [see Figs. 6(a) and 6(b)]. When the coupling is even further increased, each of the cones closest to the M points splits into three cones [see Fig. 6(c) for a sketch of the situation].

B. External Rashba SOC

As for the internal Rashba SOC, we first discuss the regimes that apply to β - and γ -graphyne. At the end,

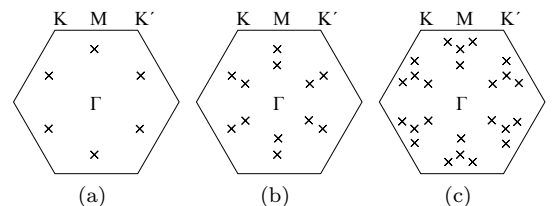


FIG. 6: Sketches of the phases corresponding to the regime $t_{\text{ext}}/t_{\text{int}} < -2^{1/3}$. Each cross denotes a Dirac cone and we have taken $t_{\text{ext}}/t_{\text{int}} = -1.3$. (a) Brillouin zone for $\lambda_{\text{int,R}} = \lambda_{\text{ext,R}} = 0$, (b) Brillouin zone for $\lambda_{\text{int,R}}/t_{\text{int}} = 0.1$ or $\lambda_{\text{ext,R}}/t_{\text{int}} = 0.1$, and (c) Brillouin zone for $\lambda_{\text{int,R}}/t_{\text{int}} = 0.4$ or $\lambda_{\text{ext,R}}/t_{\text{int}} = 0.8$.

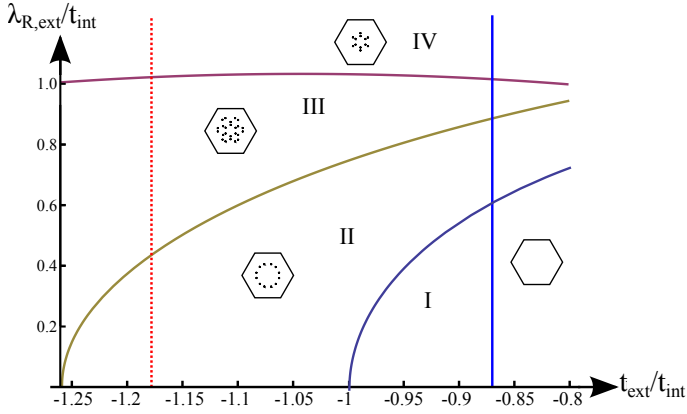


FIG. 7: (Color online) Phase diagram for the effective Hamiltonian (51) with external Rashba SOC. Region I corresponds to a gapped system, region II exhibits six pairs of Dirac cones along a line perpendicular to the line connecting Γ and M , region III exhibits six Dirac cones along a line perpendicular to the line connecting Γ and M , and six pairs of Dirac cones along the lines connecting Γ and M , and region IV shows the system with only six pairs of Dirac cones along the line connecting Γ and M .

we shortly comment on the other regimes. The relevant phase diagram is shown in Fig. 7, where again the red dashed line corresponds to β -graphyne and the blue solid line corresponds to γ -graphyne.

First, we consider the regime $-1.26 < t_{ext}/t_{int} < -1$ that applies to β -graphyne. Initially, the system exhibits six Dirac cones along the lines connecting the Γ and M points. As the external Rashba SOC is switched on, each of these Dirac cones splits into a pair of Dirac cones located along lines perpendicular to the line connecting the Γ and M points (see region II in Fig. 7). At an intermediate value of the external Rashba SOC parameter, six additional pairs of Dirac cones emerge, located along the lines connecting the Γ and M points. When the coupling is even further increased, the pairs perpendicular to the lines connecting the Γ and M points eventually merge and vanish along the lines connecting the K (K') and Γ points (see region IV in Fig. 7).

We now move on to discuss the case $-1 < t_{ext}/t_{int} < -0.8$, the relevant regime for γ -graphyne. For $-1 < t_{ext}/t_{int}$ the system is gapped, and remains to be such for small values of the external Rashba SOC (see region I in Fig. 7). However, at an intermediate value of the coupling, six pairs of Dirac cones emerge along the line connecting the K and K' points (see region II in Fig. 7). For increasing values of the coupling parameter γ -graphyne undergoes the same phase transitions as β -graphyne. Hence, subsequently it will enter regions III and IV (see Fig. 7). Finally, in the regime $-2 < t_{ext}/t_{int} < -1.26$ (not shown in Fig. 7) the external Rashba SOC acts in the same way as the internal Rashba SOC does (see also Fig. 6).

C. Interplay between internal and external Rashba spin-orbit coupling

Since in real graphynes both the internal and external Rashba SOC are present simultaneously, we now consider this case. Inspection of Table IV shows that the internal Rashba SOC parameter $\lambda_{ext,R}$ has an opposite sign compared to $\lambda_{int,R}$. As a result, we study the case where the two parameters have opposite sign, and for simplicity we set their magnitudes to be equal. The relevant phase diagram is shown in Fig. 8. We observe that this phase diagram with both couplings looks almost identical to the one for internal Rashba SOC only (compare Figs. 5 and 8). However, there are some distinct features in the phase diagram containing both couplings. First of all, in Fig. 5 the red (dashed) line, corresponding to β -graphyne crosses region II, whereas in Fig. 8 this line crosses region IV. Hence, in this particular setup, the Rashba SOC does not open a gap in β -graphyne. Moreover, the line separating phases III and IV exhibits a cusp around $t_{ext}/t_{int} = -1.25$. It turns out that to the right of this cusp the Dirac cones merge along the lines connecting K and K' points, whereas to the left of this cusp the Dirac cones annihilate along the lines connecting K and Γ points. It should be noted that this latter behavior was also observed in the presence of external Rashba SOC (see Fig. 7). Most importantly, this shows that upon including both couplings the phase diagram interpolates between the cases when only one of the couplings is present (see Figs. 5 and 7).

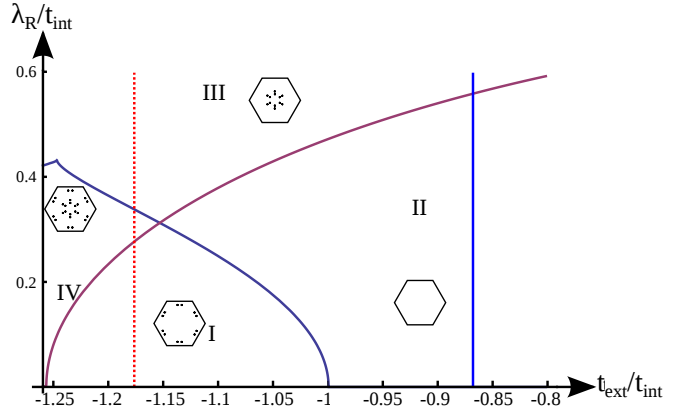


FIG. 8: (Color online) Phase diagram for the effective Hamiltonian (51) with internal and external Rashba SOC, where $\lambda_R = \lambda_{ext,R} = -\lambda_{int,R}$. In region I the system exhibits 12 Dirac cones, region II corresponds to the gapped phase, region III corresponds to the system where only pairs of Dirac cones along the line Γ - M are present, and region IV corresponds to a system where there are six pairs of cones along the line Γ - M and six pairs on lines perpendicular to Γ - M .

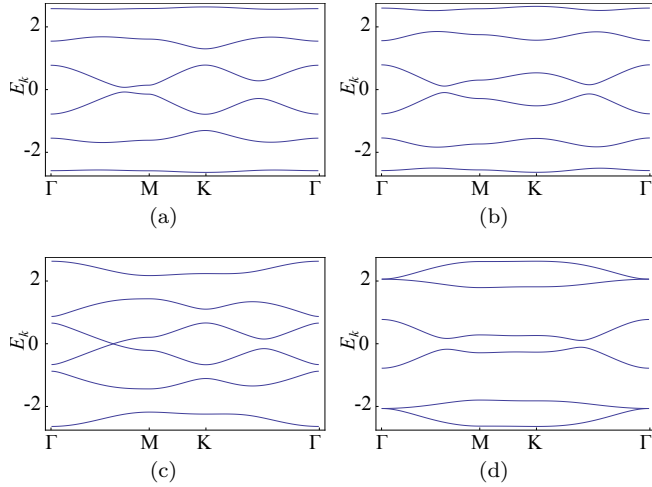


FIG. 9: (Color online) Band structure for β -graphyne for different values of $\lambda_{\text{int},I}$ and $\lambda_{\text{ext},I}$, along the line $k_x = 0$. (a) $\lambda_{\text{ext},I} = 0.15\text{eV}$ and $\lambda_{\text{int},I} = 0\text{eV}$. (b) $\lambda_{\text{ext},I} = 0\text{eV}$ and $\lambda_{\text{int},I} = 0.3\text{eV}$. (c) $\lambda_{\text{ext},I} = 0.15\text{eV}$ and $\lambda_{\text{int},I} = 0.3\text{eV}$. (d) $\lambda_{\text{ext},I} = 0.15\text{eV}$ and $\lambda_{\text{int},I} = -0.3\text{eV}$.

D. Intrinsic spin-orbit coupling

Whereas the internal and external Rashba SOC lead to a qualitative difference in the band structure, such a difference is absent when studying the intrinsic SOC. It is found that if the system exhibits Dirac cones, i.e. $-2 < t_{\text{ext}}/t_{\text{int}} < -1$, both the internal and external intrinsic SOC open the gap located between the Γ and M points [see Figs. 9(a) and 9(b)], that turns out to be topologically nontrivial [24]. However, if we combine both internal and external intrinsic SOC, both the magnitudes and the signs of the couplings $\lambda_{\text{int},I}$ and $\lambda_{\text{ext},I}$ play an important role. It turns out that if both couplings have the same sign, the two contributions tend to cancel each other, see Fig. 9(c). On the other hand, if both couplings have opposite sign, the two contributions enhance the gap located at the line connecting the Γ and M points, see Fig. 9(d).

Although at first sight it might be surprising that for opposite sign of the coupling parameters $\lambda_{\text{int},I}$ and $\lambda_{\text{ext},I}$ the gap is enhanced, this results from the fact that we have eliminated the p_z -orbitals located at the edges. For β -graphyne with orbitals at the edges included, the intrinsic SOC is governed by the coupling parameters $\lambda_{I,2}$ and $\lambda_{I,3}$ that have both the same sign, see Table II. Then, if we eliminate the p_z -orbitals located at the edges, the intrinsic SOC is governed by the coupling parameters $\lambda_{\text{int},I}$ and $\lambda_{\text{ext},I}$. However, inspection of Table IV tells us that the coupling parameter describing the internal intrinsic SOC has an overall minus sign, whereas the external intrinsic SOC has not. Hence, a sign difference in the value for the parameters $\lambda_{\text{int},I}$ and $\lambda_{\text{ext},I}$ corresponds to the situation that in the full model, containing both orbitals at edges and vertices, the parameters $\lambda_{I,2}$ and $\lambda_{I,3}$ have the

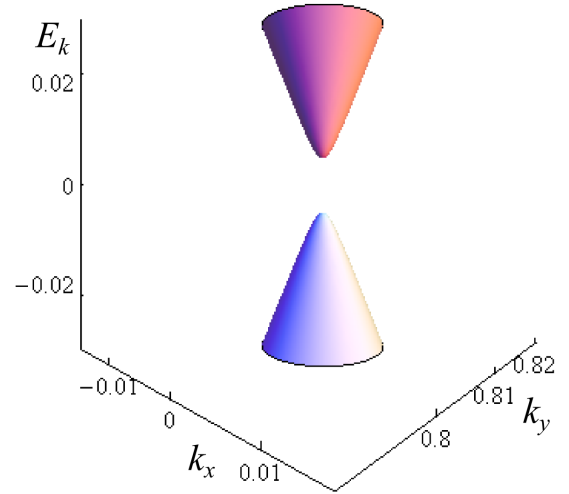


FIG. 10: (Color online) Topological band gap opening at the K -point in α -graphyne due to the intrinsic SOC, for $\lambda_I \approx 0.05\text{eV}$.

same sign.

V. DISCUSSION AND CONCLUSIONS

Let us now apply the obtained general results to α - and γ -graphyne.

α -graphyne with SOC is effectively described by the same Hamiltonian as graphene [see Eqs. (2), (46), and (47)]. As a result, for an arbitrary non-zero value of the intrinsic SOC parameter λ_I a topological band gap opens [2]. The intrinsic SOC opens a non-trivial gap, but respects the spin degeneracy (see Fig. 10). The

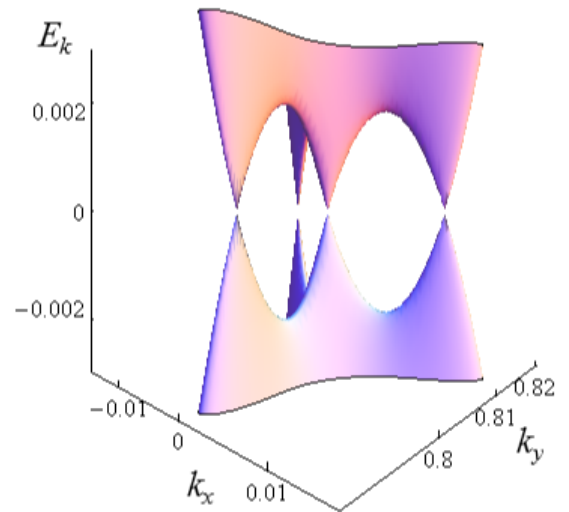


FIG. 11: (Color online) Band structure for α -graphyne including the Rashba SOC for $\lambda_R \approx 0.5\text{eV}$, zoomed in on the K point.

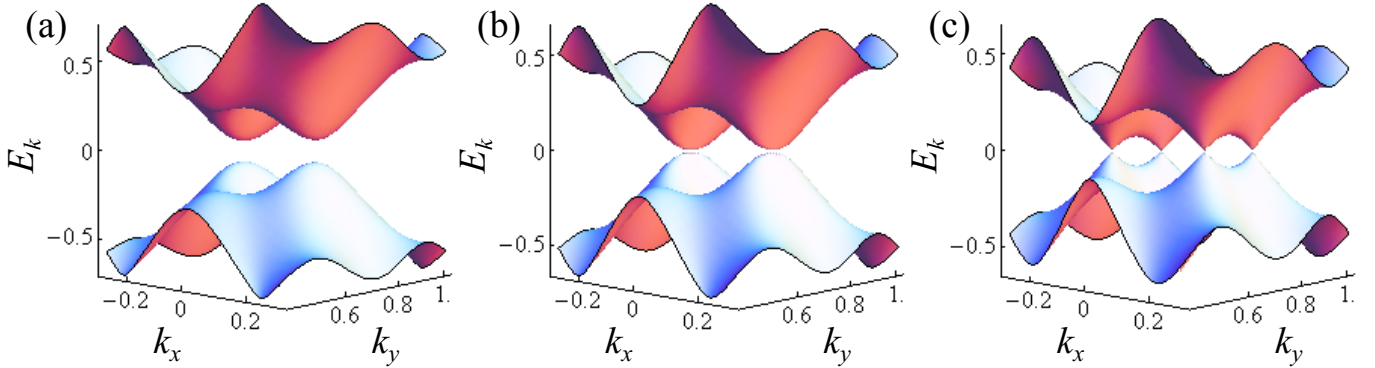


FIG. 12: (Color online) Band structure of γ -graphyne in the presence of external Rashba SOC, zoomed in on the M-point in the BZ. (a) Gapped system, for $\lambda_{\text{ext,R}} \approx 0.9\text{eV}$, (b) transition from gapped system into a zero-gap semiconductor, for $\lambda_{\text{ext,R}} \approx 1.04\text{eV}$, and (c) two pairs of Dirac cones, for $\lambda_{\text{ext,R}} \approx 1.2\text{eV}$.

Rashba SOC leads to trigonal warping and lifts the spin-degeneracy [28,29] (see also Fig. 11). When both Rashba and intrinsic SOC are present, the spin-degeneracy is lifted, the electron-hole symmetry is broken, and the Rashba SOC tends to close the gap induced by the intrinsic SOC. The main difference compared to graphene is the reduced Fermi velocity and the larger band gap due to the stronger intrinsic SOC in graphynes. Note that the SOC in graphene has been extensively studied by means of first-principles calculations (see Refs. [30–33]).

Whereas β -graphyne exhibits Dirac cones and the Rashba SOC can destroy the Dirac behavior by opening a gap when the cones merge [24], we find that in γ -graphyne the situation is completely reversed. First of all, we note that in γ -graphyne the external SOC dominates, simply because by hopping through the acetylene bond one can flip the spin three times as many as compared to hopping through the single bond. The relevant phase diagram is given in Fig. 7. When the coupling parameter $\lambda_{\text{ext,R}}$ is increased, six new pairs emerge along the line connecting K and K' (see region II in Figs. 7 and 12). As the coupling parameter is further increased, we find that six additional pairs of Dirac cones emerge on the line connecting the Γ and M points (see region III in Fig. 7). Merging of the Dirac cones and the corresponding gap opening in shaken honeycomb optical lattices have been recently studied in Ref. [34].

To summarize, in this paper we have developed a tight-binding theory for the spin-orbit couplings in graphynes. For completeness, we first considered α -, β -, and γ -graphyne in absence of the SOC. An effective description in terms of only p_z -orbitals captures their bandstructures quite well. To describe the SOC, besides the p_z -orbitals, we have included the σ - and d -orbitals, as these two sets of orbitals are now coupled. At half-filling, the latter are away from the Fermi level, and we have integrated them out to obtain an effective TB model in terms of only p_z orbitals at both edges and vertices. In the last step, the orbitals at the edges have been eliminated and an effective TB model in terms of only orbitals

at vertices has been obtained. We have then studied the effective TB models for α - and γ -graphynes, and have repeated some of the results for β -graphyne, previously published in Ref. [24], however now in the context of this general theory.

As a result, the effective low-energy description of α -graphyne differs from graphene with respect to the value of the SOC, and the effective NN-hopping parameter. With respect to β - and γ -graphyne, we find that we have to distinguish between external and internal SOC. In all the three compounds, the effect of the d -orbitals is to increase the value of the SOC parameters. We expect that the internal Rashba SOC dominates in β -graphyne. By tuning an applied electric field, the system can become gapped. On the other hand, for γ -graphyne we expect that the external SOC is dominant, and the gap can be closed by applying an electric field. Concerning the intrinsic SOC, we would like to point out that the internal and external SOC can compete with each other. As already shown in Ref. [24], in β -graphyne the intrinsic SOC opens a non-trivial gap. On the other hand, in γ -graphyne the bandgap is topologically trivial, and we estimate that for realistic values of the SOC it cannot be turned into a topological one. We hope that our findings will be a useful base for studying the SOC-related phenomena in other graphynes, such as 6, 6, 12- and δ -graphyne [17]. Finally, we also anticipate that our results will motivate further *ab initio* studies of the SOC in graphynes.

VI. ACKNOWLEDGMENTS

We would like to thank D. S. Galvão for fruitful discussions. This work is part of the D-ITP consortium, a program of the Netherlands Organization for Scientific Research (NWO) that is funded by the Dutch Ministry of Education, Culture and Science (OCW). The authors acknowledge financial support from NWO and the Dutch FOM association with the program "Designing Dirac car-

riers in semiconductor honeycomb lattices”.

Appendix A: Low energy tight-binding Hamiltonian

Here, we outline the method used in this paper to derive effective Hamiltonians. Consider a system where we can split the spinor Ψ into a high-energy component Ψ_h and a low-energy component Ψ_l . Then, we may write the Hamiltonian matrix in a block form

$$H(\mathbf{k}) = \begin{pmatrix} H_{ll}(\mathbf{k}) & H_{lh}(\mathbf{k}) \\ H_{lh}^\dagger(\mathbf{k}) & H_{hh}(\mathbf{k}) \end{pmatrix}. \quad (\text{A1})$$

Using this decomposition, the Schrödinger equation reads as

$$E\Psi_l(\mathbf{k}) = H_{ll}(\mathbf{k})\Psi_l(\mathbf{k}) + H_{lh}(\mathbf{k})\Psi_h(\mathbf{k}) \quad (\text{A2})$$

$$E\Psi_h(\mathbf{k}) = H_{lh}^\dagger(\mathbf{k})\Psi_l(\mathbf{k}) + H_{hh}(\mathbf{k})\Psi_h(\mathbf{k}). \quad (\text{A3})$$

We can then use Eq. (A3) to eliminate $\Psi_h(\mathbf{k})$ in Eq. (A2). Since $H_{lh}^\dagger(\mathbf{k})\Psi_l(\mathbf{k}) = (-H_{hh}(\mathbf{k}) + E)\Psi_h(\mathbf{k})$, up to first order in E we obtain $\Psi_h(\mathbf{k}) = -H_{hh}^{-1}(\mathbf{k})(1 + EH_{hh}^{-1}(\mathbf{k}))H_{lh}^\dagger(\mathbf{k})\Psi_l(\mathbf{k})$. Therefore, Eq. (A2) reduces to

$$(H_{ll}(\mathbf{k}) - H_{lh}(\mathbf{k})H_{hh}^{-1}(\mathbf{k})H_{lh}^\dagger(\mathbf{k}))\Psi_l(\mathbf{k}) = E(\mathbb{I} + H_{lh}(\mathbf{k})H_{hh}^{-2}(\mathbf{k})H_{lh}^\dagger(\mathbf{k}))\Psi_l(\mathbf{k}). \quad (\text{A4})$$

If we now introduce $S(\mathbf{k}) = \mathbb{I} + H_{lh}(\mathbf{k})H_{hh}^{-2}(\mathbf{k})H_{lh}^\dagger(\mathbf{k})$, and define $\phi(\mathbf{k}) = S^{1/2}(\mathbf{k})\Psi_l(\mathbf{k})$, we find the eigenvalue equation

$$(H_{ll}(\mathbf{k}) - H_{lh}(\mathbf{k})H_{hh}^{-1}(\mathbf{k})H_{lh}^\dagger(\mathbf{k}))S^{-1/2}(\mathbf{k})\phi(\mathbf{k}) = ES^{1/2}(\mathbf{k})\phi(\mathbf{k}). \quad (\text{A5})$$

By multiplying Eq. (A5) on both sides with $S^{-1/2}(\mathbf{k})$ we find

$$H_{\text{eff}}(\mathbf{k})\phi(\mathbf{k}) = E\phi(\mathbf{k}), \quad (\text{A6})$$

with $H_{\text{eff}}(\mathbf{k})$ given by

$$H_{\text{eff}}(\mathbf{k}) = S^{-1/2}(\mathbf{k})(H_{ll}(\mathbf{k}) - H_{lh}(\mathbf{k})H_{hh}^{-1}(\mathbf{k})H_{lh}^\dagger(\mathbf{k}))S^{-1/2}(\mathbf{k}) \quad (\text{A7})$$

In various cases we consider in this paper the matrix S happens to be diagonal, which greatly simplifies the expressions. It turns out that we can Fourier transform the effective Hamiltonian back to real space, and obtain an effective real space Hamiltonian. Note that several papers adopt a different approach, where they write down the transfer equations, then integrate out the high-energy contributions, see for example Ref. [18]. The drawback of their method lies in the fact that this can lead to a non-Hermitian Hamiltonian, as it happens for example in the context of 6, 6, 12-graphyne [25].

Appendix B: Effective Hamiltonian without spin-orbit coupling

In the main text, we have pointed out that the orbitals located at the vertices correspond to the low-energy states, whereas the orbitals at the edges give rise to high-energy states. This can be seen from the relation $|t_1| < |t_2| < |t_3|$, because the vertices are coupled by the parameter t_3 , whereas the edges are coupled by the parameter t_2 . Therefore, we can apply the low-energy approximation to the graphynes we consider, and we are able to accurately describe α -graphyne in terms of a two-site model, and β - and γ -graphyne by a six-site model. In the following, we make use of three normalized NN vectors \mathbf{d}_i , $i = 1, 2, 3$ given by

$$\begin{aligned} \mathbf{d}_1 &= (-1/2, \sqrt{3}/2), \\ \mathbf{d}_2 &= (1, 0) \\ \mathbf{d}_3 &= (-1/2, -\sqrt{3}/2). \end{aligned} \quad (\text{B1})$$

We denote the different bond lengths by l_i , $i = 1, 2, 3$, corresponding to the vertex-vertex, vertex-edge, and edge-edge bonds, respectively. Furthermore, we define $l_4 = 2l_2 + l_3$.

1. Effective Hamiltonian for α -graphyne

By performing a Fourier transformation on Eq. (1) we obtain

$$H^\alpha = \int dk \Psi^\dagger(\mathbf{k}) H(\mathbf{k}) \Psi(\mathbf{k}),$$

where $H(\mathbf{k})$ is given by Eq. (A1),

$$\Psi(k) = (A(\mathbf{k}), B(\mathbf{k}), a^1(\mathbf{k}), a^2(\mathbf{k}), a^3(\mathbf{k}), b^1(\mathbf{k}), b^2(\mathbf{k}), b^3(\mathbf{k}))^T, \quad (\text{B2})$$

and $H_{ll}(\mathbf{k})$, $H_{lh}(\mathbf{k})$, and $H_{hh}(\mathbf{k})$ are given by

$$\begin{aligned} H_{ll}(\mathbf{k}) &= 0, \\ H_{lh}(\mathbf{k}) &= t_{\alpha,1} \begin{pmatrix} e^{il_2\mathbf{k}\cdot\mathbf{d}_1} & e^{il_2\mathbf{k}\cdot\mathbf{d}_2} & e^{il_2\mathbf{k}\cdot\mathbf{d}_3} & 0 & 0 & 0 \\ 0 & 0 & 0 & e^{-il_2\mathbf{k}\cdot\mathbf{d}_1} & e^{-il_2\mathbf{k}\cdot\mathbf{d}_2} & e^{-il_2\mathbf{k}\cdot\mathbf{d}_3} \end{pmatrix}, \\ H_{hh}(\mathbf{k}) &= t_{\alpha,2} \begin{pmatrix} 0 & \text{diag}(e^{il_3\mathbf{k}\cdot\mathbf{d}_1}, e^{il_3\mathbf{k}\cdot\mathbf{d}_2}, e^{il_3\mathbf{k}\cdot\mathbf{d}_3}) \\ \text{diag}(e^{-il_3\mathbf{k}\cdot\mathbf{d}_1}, e^{-il_3\mathbf{k}\cdot\mathbf{d}_2}, e^{-il_3\mathbf{k}\cdot\mathbf{d}_3}) & 0 \end{pmatrix}. \end{aligned}$$

If we now follow the method outlined in Appendix A, we obtain

$$(H_{ll}(\mathbf{k}) - H_{lh}(\mathbf{k}) H_{hh}^{-1}(\mathbf{k}) H_{lh}^\dagger(\mathbf{k})) = -\frac{t_{\alpha,1}^2}{t_{\alpha,2}} \begin{pmatrix} 0 & f(\mathbf{k}) \\ f^*(\mathbf{k}) & 0 \end{pmatrix},$$

with $f(\mathbf{k}) = \sum_{j=1}^3 e^{i\mathbf{k}\cdot\mathbf{d}_j l_4}$, and S is given by

$$S = \mathbb{I}(1 + 3t_{\alpha,1}^2/t_{\alpha,2}^2)$$

. Hence, the effective Hamiltonian reads as

$$H_{\text{eff}}^\alpha(\mathbf{k}) = -\frac{t_{\alpha,1}^2 t_{\alpha,2}}{t_{\alpha,2}^2 + 3t_{\alpha,1}^2} \begin{pmatrix} 0 & f(\mathbf{k}) \\ f^*(\mathbf{k}) & 0 \end{pmatrix},$$

and leads to Eq. (2) after performing an inverse Fourier transformation to obtain the real-space Hamiltonian.

2. Effective Hamiltonian for β -graphyne

In momentum space the Hamiltonian Eq. (3) reads as

$$H^\beta = \int dk \Psi^\dagger(\mathbf{k}) H(\mathbf{k}) \Psi(\mathbf{k}),$$

where $H(\mathbf{k})$ is given by Eq. (A1),

$$\begin{aligned} \Psi(\mathbf{k}) &= (A(\mathbf{k}), B(\mathbf{k}), C(\mathbf{k}), D(\mathbf{k}), E(\mathbf{k}), F(\mathbf{k}), a^1(\mathbf{k}), b^1(\mathbf{k}), c^1(\mathbf{k}), d^1(\mathbf{k}), e^1(\mathbf{k}), f^1(\mathbf{k}), \\ &\quad a^2(\mathbf{k}), b^2(\mathbf{k}), c^2(\mathbf{k}), d^2(\mathbf{k}), e^2(\mathbf{k}), f^2(\mathbf{k}))^T. \end{aligned}$$

Here, $H_{ll}(\mathbf{k})$ is given by

$$H_{ll}(\mathbf{k}) = t_{\beta,1} \begin{pmatrix} 0 & \text{diag}(e^{i\mathbf{k}\cdot\mathbf{d}_1 l_1}, e^{-i\mathbf{k}\cdot\mathbf{d}_2 l_1}, e^{i\mathbf{k}\cdot\mathbf{d}_3 l_1}) \\ \text{diag}(e^{-i\mathbf{k}\cdot\mathbf{d}_1 l_1}, e^{i\mathbf{k}\cdot\mathbf{d}_2 l_1}, e^{-i\mathbf{k}\cdot\mathbf{d}_3 l_1}) & 0 \end{pmatrix}.$$

The matrix $H_{lh}(\mathbf{k})$, which couples electrons at the vertices to the electrons belonging to the acetylene linkage, can be further decomposed as

$$H_{lh}(\mathbf{k}) = t_{\beta,2} \begin{pmatrix} H_{lh}^1(\mathbf{k}) & H_{lh}^2(\mathbf{k}) \end{pmatrix},$$

where $H_{lh}^1(\mathbf{k})$ and $H_{lh}^2(\mathbf{k})$ read

$$\begin{aligned} H_{lh}^1(\mathbf{k}) &= \text{diag}(e^{i\mathbf{k}\cdot\mathbf{d}_3l_2}, e^{-i\mathbf{k}\cdot\mathbf{d}_3l_2}, e^{i\mathbf{k}\cdot\mathbf{d}_2l_2}, e^{-i\mathbf{k}\cdot\mathbf{d}_2l_2}, e^{i\mathbf{k}\cdot\mathbf{d}_1l_2}, e^{-i\mathbf{k}\cdot\mathbf{d}_1l_2}), \\ H_{lh}^2(\mathbf{k}) &= \text{diag}(e^{i\mathbf{k}\cdot\mathbf{d}_2l_2}, e^{-i\mathbf{k}\cdot\mathbf{d}_1l_2}, e^{i\mathbf{k}\cdot\mathbf{d}_1l_2}, e^{-i\mathbf{k}\cdot\mathbf{d}_3l_2}, e^{i\mathbf{k}\cdot\mathbf{d}_3l_2}, e^{-i\mathbf{k}\cdot\mathbf{d}_2l_2}). \end{aligned}$$

Finally, we decompose the matrix $H_{hh}(\mathbf{k})$ as

$$H_{hh}(\mathbf{k}) = t_{\beta,3} \begin{pmatrix} H_1(\mathbf{k}) & 0 \\ 0 & H_2(\mathbf{k}) \end{pmatrix}.$$

The matrices $H_1(\mathbf{k})$ and $H_2(\mathbf{k})$ are given by

$$H_1(\mathbf{k}) = \text{diag}(U_3(\mathbf{k}), U_2(\mathbf{k}), U_1(\mathbf{k})),$$

$$H_2(\mathbf{k}) = \begin{pmatrix} 0 & 0 & 0 & e^{i\mathbf{k}\cdot\mathbf{d}_2l_3} \\ 0 & U_1(-\mathbf{k}) & 0 & 0 \\ 0 & 0 & U_3(-\mathbf{k}) & 0 \\ e^{-i\mathbf{k}\cdot\mathbf{d}_2l_3} & 0 & 0 & 0 \end{pmatrix},$$

with

$$U_i(\mathbf{k}) = \begin{pmatrix} 0 & e^{i\mathbf{k}\cdot\mathbf{d}_il_3} \\ e^{-i\mathbf{k}\cdot\mathbf{d}_il_3} & 0 \end{pmatrix}.$$

If we now perform the low-energy approximation, we find that $S = (1 + 2t_{\beta,2}^2/t_{\beta,3}^2)\mathbb{I}$. Furthermore, if we change the basis to $\tilde{\Psi} = (A, C, E, B, D, F)$, then $H_{ll}(\mathbf{k}) - H_{lh}(\mathbf{k})H_{hh}^{-1}(\mathbf{k})H_{lh}^\dagger(\mathbf{k})$ reads

$$H_{ll}(\mathbf{k}) - H_{lh}(\mathbf{k})H_{hh}^{-1}(\mathbf{k})H_{lh}^\dagger(\mathbf{k}) = \begin{pmatrix} 0 & U(\mathbf{k}) \\ U^\dagger(\mathbf{k}) & 0 \end{pmatrix},$$

and $U(\mathbf{k})$ reads

$$U(\mathbf{k}) = \begin{pmatrix} \frac{t_{\beta,2}^2}{t_{\beta,3}} e^{i\mathbf{k}\cdot\mathbf{d}_3l_4} & t_{\beta,1} e^{i\mathbf{k}\cdot\mathbf{d}_1l_1} & \frac{t_{\beta,2}^2}{t_{\beta,3}} e^{i\mathbf{k}\cdot\mathbf{d}_2l_4} \\ \frac{t_{\beta,2}^2}{t_{\beta,3}} e^{i\mathbf{k}\cdot\mathbf{d}_1l_4} & \frac{t_{\beta,2}^2}{t_{\beta,3}} e^{i\mathbf{k}\cdot\mathbf{d}_2l_4} & t_{\beta,1} e^{i\mathbf{k}\cdot\mathbf{d}_3l_1} \\ t_{\beta,1} e^{i\mathbf{k}\cdot\mathbf{d}_2l_1} & \frac{t_{\beta,2}^2}{t_{\beta,3}} e^{i\mathbf{k}\cdot\mathbf{d}_3l_4} & \frac{t_{\beta,2}^2}{t_{\beta,3}} e^{i\mathbf{k}\cdot\mathbf{d}_1l_4} \end{pmatrix}.$$

If we perform an inverse Fourier transformation, we obtain Eq. (4), the real-space β -graphyne Hamiltonian.

3. Effective Hamiltonian for γ -graphyne

By applying a Fourier transformation on Eq. (5), we obtain

$$H^\gamma = \int d\mathbf{k} \Psi^\dagger(\mathbf{k}) H(\mathbf{k}) \Psi(\mathbf{k}),$$

where $H_{\mathbf{k}}$ is given by Eq. (A1), and

$$\Psi(\mathbf{k}) = (A(\mathbf{k}), C(\mathbf{k}), E(\mathbf{k}), B(\mathbf{k}), D(\mathbf{k}), F(\mathbf{k}), a(\mathbf{k}), c(\mathbf{k}), e(\mathbf{k}), b(\mathbf{k}), d(\mathbf{k}), f(\mathbf{k}))^T.$$

The matrix $H_{ll}(\mathbf{k})$ reads

$$H_{ll}(\mathbf{k}) = t_{\gamma,1} \begin{pmatrix} 0 & U_{ll}(\mathbf{k}) \\ U_{ll}^\dagger(\mathbf{k}) & 0 \end{pmatrix},$$

with $U_l(\mathbf{k})$ given by

$$U_l(\mathbf{k}) = \begin{pmatrix} e^{i\mathbf{k}\cdot\mathbf{d}_3l_1} & 0 & e^{i\mathbf{k}\cdot\mathbf{d}_2l_1} \\ e^{i\mathbf{k}\cdot\mathbf{d}_1l_1} & e^{i\mathbf{k}\cdot\mathbf{d}_2l_1} & 0 \\ 0 & e^{i\mathbf{k}\cdot\mathbf{d}_3l_1} & e^{i\mathbf{k}\cdot\mathbf{d}_1l_1} \end{pmatrix}.$$

Furthermore, we find

$$H_{lh} = t_{\gamma,2} \text{diag}(e^{i\mathbf{k}\cdot\mathbf{d}_1l_2}, e^{-i\mathbf{k}\cdot\mathbf{d}_2l_2}, e^{i\mathbf{k}\cdot\mathbf{d}_3l_2}, e^{-i\mathbf{k}\cdot\mathbf{d}_1l_2}, e^{i\mathbf{k}\cdot\mathbf{d}_2l_2}, e^{-i\mathbf{k}\cdot\mathbf{d}_3l_2}).$$

Finally, $H_{hh}(\mathbf{k})$ reads

$$H_{hh}(\mathbf{k}) = t_{\gamma,3} \begin{pmatrix} 0 & \text{diag}(e^{i\mathbf{k}\cdot\mathbf{d}_1l_3}, e^{-i\mathbf{k}\cdot\mathbf{d}_2l_3}, e^{i\mathbf{k}\cdot\mathbf{d}_3l_3}) \\ \text{diag}(e^{-i\mathbf{k}\cdot\mathbf{d}_1l_3}, e^{i\mathbf{k}\cdot\mathbf{d}_2l_3}, e^{-i\mathbf{k}\cdot\mathbf{d}_3l_3}) & 0 \end{pmatrix},$$

Therefore, we find $S = (1 + t_{\gamma,2}^2/t_{\gamma,3}^2)\mathbb{I}$, and

$$H_u(\mathbf{k}) - H_{lh}(\mathbf{k})H_{hh}^{-1}(\mathbf{k})H_{lh}^\dagger(\mathbf{k}) = \begin{pmatrix} 0 & U(\mathbf{k}) \\ U^\dagger(\mathbf{k}) & 0 \end{pmatrix},$$

with

$$U(\mathbf{k}) = \begin{pmatrix} t_{\gamma_1} e^{i\mathbf{k}\cdot\mathbf{d}_3l_4} & \frac{-t_{\gamma,2}^2}{t_{\gamma,3}} e^{i\mathbf{k}\cdot\mathbf{d}_1l_1} & t_{\gamma_1} e^{i\mathbf{k}\cdot\mathbf{d}_2l_4} \\ t_{\gamma_1} e^{i\mathbf{k}\cdot\mathbf{d}_1l_4} & t_{\gamma_1} e^{i\mathbf{k}\cdot\mathbf{d}_2l_4} & \frac{-t_{\gamma,2}^2}{t_{\gamma,3}} e^{i\mathbf{k}\cdot\mathbf{d}_3l_1} \\ \frac{-t_{\gamma,2}^2}{t_{\gamma,3}} e^{i\mathbf{k}\cdot\mathbf{d}_2l_1} & t_{\gamma_1} e^{i\mathbf{k}\cdot\mathbf{d}_3l_4} & t_{\gamma_1} e^{i\mathbf{k}\cdot\mathbf{d}_1l_4} \end{pmatrix}.$$

As a result, after an inverse Fourier transformation, we end up with the effective Hamiltonian Eq. (6).

Appendix C: σ -tight-binding models

In this appendix we present the TB models containing σ -orbitals, used to derive the SOC Hamiltonians. To denote different σ -orbitals on each site, we introduce a subscript $j = 1, 2, 3$. Different sites are labeled by a superscript (the same as for p_z -orbitals), see Fig. 1.

1. σ -tight-binding model for α -graphyne

The labeling of the different σ -orbitals is shown in Fig. 13. Combining this labeling with the definition of the dominant NN hoppings (V_2, V_3, V_4) as given in Fig. 4(a), we find that H_{NN}^α reads

$$\begin{aligned} H_{NN}^\alpha = & V_2 \sum_{\langle i,j \rangle} \left(A_{1,i}^\dagger a_{1,j}^1 + A_{2,i}^\dagger a_{2,j}^2 + A_{3,i}^\dagger a_{3,j}^3 + B_{1,i}^\dagger b_{1,j}^1 + B_{2,i}^\dagger b_{2,j}^2 + B_{3,i}^\dagger b_{3,j}^3 \right) + V_3 \sum_{\langle i,j \rangle} [(a_{3,i}^1)^\dagger b_{3,j}^1 + (a_{2,i}^2)^\dagger b_{2,j}^2 \\ & + (a_{2,i}^3)^\dagger b_{2,j}^3] + V_4 \sum_{\langle i,j \rangle} [(a_{2,i}^1)^\dagger b_{2,j}^1 + (a_{3,i}^2)^\dagger b_{3,j}^2 + (a_{1,i}^3)^\dagger b_{1,j}^3] + h.c. \end{aligned} \quad (\text{C1})$$

The on-site energies ($\varepsilon_2, \varepsilon_3, \varepsilon_4$) and hoppings (V_6, V_9) are included in H_{onsite}^α , which is given by

$$\begin{aligned} H_{\text{onsite}}^\alpha = & \frac{\varepsilon_2}{2} \sum_i \left(A_{1,i}^\dagger A_{1,i} + A_{2,i}^\dagger A_{2,i} + A_{3,i}^\dagger A_{3,i} + B_{1,i}^\dagger B_{1,i} + B_{2,i}^\dagger B_{2,i} + B_{3,i}^\dagger B_{3,i} \right) \\ & + \frac{\varepsilon_3}{2} \sum_i [(a_{3,i}^1)^\dagger a_{3,i}^1 + (a_{2,i}^2)^\dagger a_{2,i}^2 + (a_2^3)^\dagger a_2^3 + (b_{3,i}^1)^\dagger b_{3,i}^1 + (b_{2,i}^2)^\dagger b_{2,i}^2 + (b_{2,i}^3)^\dagger b_{2,i}^3] \\ & + \frac{\varepsilon_4}{2} \sum_i [(a_{1,i}^1)^\dagger a_{1,i}^1 + (a_{2,i}^2)^\dagger a_{2,i}^2 + (a_{3,i}^3)^\dagger a_{3,i}^3 + (b_{1,i}^1)^\dagger b_{1,i}^1 + (b_{2,i}^2)^\dagger b_{2,i}^2 + (b_{3,i}^3)^\dagger b_{3,i}^3] \\ & + V_6 \sum_i \left(A_{1,i}^\dagger A_{2,i} + A_{2,i}^\dagger A_{3,i} + A_{3,i}^\dagger A_{1,i} + B_{1,i}^\dagger B_{2,i} + B_{2,i}^\dagger B_{3,i} + B_{3,i}^\dagger B_{1,i} \right) \\ & + V_9 \sum_i [(a_{1,i}^1)^\dagger a_{3,i}^1 + (a_{2,i}^2)^\dagger a_{2,i}^2 + (a_{3,i}^3)^\dagger a_{2,i}^3 + (b_{1,i}^1)^\dagger b_{3,i}^1 + (b_{2,i}^2)^\dagger b_{1,i}^2 + (b_{3,i}^3)^\dagger b_{2,i}^3] + h.c. \end{aligned} \quad (\text{C2})$$

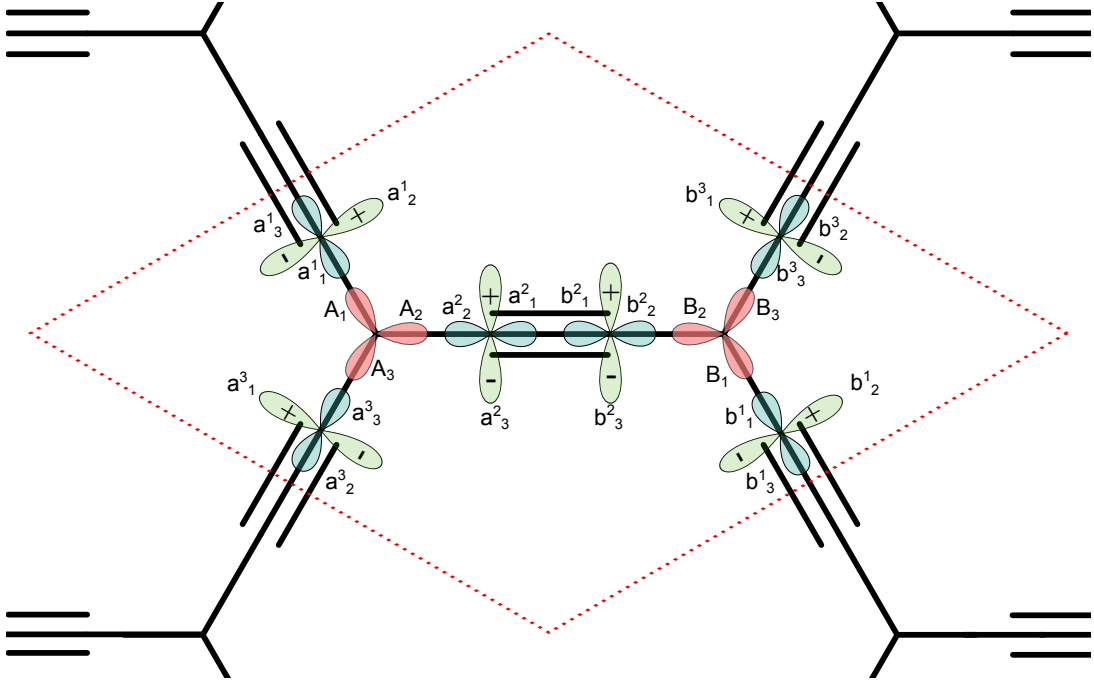


FIG. 13: (Color online) Labeling used for the α -graphyne TB model.

2. σ -tight-binding model for β -graphyne

The labeling of the different σ -orbitals is shown in Fig. 14, together with the definition of the dominant NN hoppings (V_1, \dots, V_4) shown in Fig. 4(b). We then find

$$\begin{aligned}
H_{\text{NN}}^\beta = & V_1 \sum_{\langle i,j \rangle} \left(A_{3,i}^\dagger D_{3,j} + B_{1,i}^\dagger E_{1,j} + C_{2,i}^\dagger F_{2,j} \right) + V_2 \sum_{\langle i,j \rangle} \left(A_{1,i}^\dagger a_{1,j}^2 + A_{2,i}^\dagger a_{2,j}^1 + B_{2,i}^\dagger b_{2,j}^1 + B_{3,i}^\dagger b_{3,j}^2 + C_{1,i}^\dagger c_{1,j}^1 \right. \\
& + C_{3,i}^\dagger c_{3,j}^2 + D_{1,i}^\dagger d_{1,j}^1 + D_{2,i}^\dagger d_{2,j}^2 + E_{2,i}^\dagger e_{2,j}^1 + E_{3,i}^\dagger e_{3,j}^1 + F_{1,i}^\dagger f_{1,j}^2 + F_{3,i}^\dagger f_{3,j}^1 \left. \right) + V_3 \sum_{\langle i,j \rangle} \left[(a_{1,i}^1)^\dagger b_{1,j}^1 + (a_{3,i}^2)^\dagger f_{3,j}^2 \right. \\
& + (c_{3,i}^1)^\dagger d_{3,j}^1 + (c_{2,i}^2)^\dagger b_{2,j}^2 + (e_{2,i}^1)^\dagger f_{2,j}^1 + (e_{1,i}^2)^\dagger d_{1,j}^1 \left. \right] + V_4 \sum_{\langle i,j \rangle} \left[(a_{3,i}^1)^\dagger b_{3,j}^1 + (a_{2,i}^2)^\dagger f_{2,j}^2 + (c_{2,i}^1)^\dagger d_{2,j}^1 \right. \\
& \left. + (c_{1,i}^2)^\dagger b_{1,j}^2 + (e_{1,i}^1)^\dagger f_{1,j}^1 + (e_{3,i}^2)^\dagger d_{3,j}^2 \right] + h.c., \tag{C3}
\end{aligned}$$

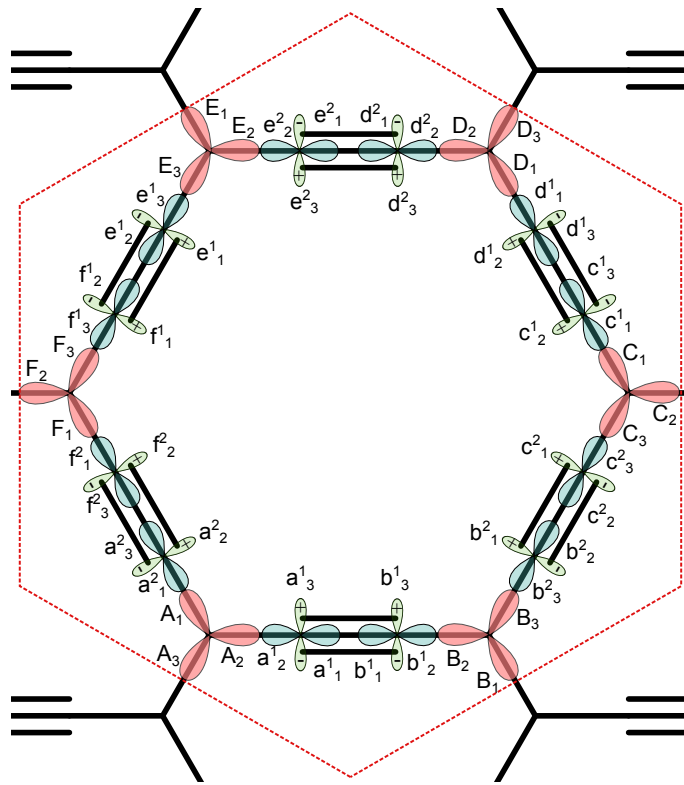


FIG. 14: (Color online) Labeling of orbitals used in the β -graphyne TB model.

The term describing the on-site energies ($\varepsilon_1, \dots, \varepsilon_5$) and hoppings (V_5, \dots, V_9) reads

$$\begin{aligned}
H_{\text{onsite}}^\beta = & \frac{\varepsilon_1}{2} \sum_i \left(A_{3,i}^\dagger A_{3,i} + B_{1,i}^\dagger B_{1,i} + C_{2,i}^\dagger C_{2,i} + D_{3,i}^\dagger D_{3,i} + E_{1,i}^\dagger E_{1,i} + F_{2,i}^\dagger F_{2,i} \right) + \frac{\varepsilon_2}{2} \sum_i \left(A_{1,i}^\dagger A_{1,i} + A_{2,i}^\dagger A_{2,i} \right. \\
& + B_{2,i}^\dagger B_{2,i} + B_{3,i}^\dagger B_{3,i} + C_{1,i}^\dagger C_{1,i} + C_{3,i}^\dagger C_{3,i} + D_{1,i}^\dagger D_{1,i} + D_{2,i}^\dagger D_{2,i} + E_{2,i}^\dagger E_{2,i} + E_{3,i}^\dagger E_{3,i} + F_{1,i}^\dagger F_{1,i} + F_{3,i}^\dagger F_{3,i} \left. \right) \\
& + \frac{\varepsilon_3}{2} \sum_i \left[(a_{1,i}^\dagger)^\dagger a_{1,i} + (a_{3,i}^\dagger)^\dagger a_{3,i} + (b_{1,i}^\dagger)^\dagger b_{1,i} + (b_{2,i}^\dagger)^\dagger b_{2,i} + (c_{3,i}^\dagger)^\dagger c_{3,i} + (c_{2,i}^\dagger)^\dagger c_{2,i} + (d_{3,i}^\dagger)^\dagger d_{3,i} + (d_{1,i}^\dagger)^\dagger d_{1,i} \right. \\
& + (e_{2,i}^\dagger)^\dagger e_{2,i} + (e_{1,i}^\dagger)^\dagger e_{1,i} + (f_{2,i}^\dagger)^\dagger f_{2,i} + (f_{3,i}^\dagger)^\dagger f_{3,i} \left. \right] + \frac{\varepsilon_4}{2} \sum_i \left[(a_{2,i}^\dagger)^\dagger a_{2,i} + (a_{1,i}^\dagger)^\dagger a_{1,i} + (b_{2,i}^\dagger)^\dagger b_{2,i} \right. \\
& + (b_{3,i}^\dagger)^\dagger b_{3,i} + (c_{1,i}^\dagger)^\dagger c_{1,i} + (c_{3,i}^\dagger)^\dagger c_{3,i} + (d_{1,i}^\dagger)^\dagger d_{1,i} + (d_{2,i}^\dagger)^\dagger d_{2,i} + (e_{3,i}^\dagger)^\dagger e_{3,i} + (e_{2,i}^\dagger)^\dagger e_{2,i} + (f_{3,i}^\dagger)^\dagger f_{3,i} + (f_{1,i}^\dagger)^\dagger f_{1,i} \left. \right] \\
& + \frac{\varepsilon_5}{2} \sum_i \left[(a_{3,i}^\dagger)^\dagger a_{3,i} + (a_{2,i}^\dagger)^\dagger a_{2,i} + (b_{3,i}^\dagger)^\dagger b_{3,i} + (b_{1,i}^\dagger)^\dagger b_{1,i} + (c_{2,i}^\dagger)^\dagger c_{2,i} + (c_{1,i}^\dagger)^\dagger c_{1,i} + (d_{2,i}^\dagger)^\dagger d_{2,i} + (d_{3,i}^\dagger)^\dagger d_{3,i} \right. \\
& + (e_{1,i}^\dagger)^\dagger e_{1,i} + (e_{3,i}^\dagger)^\dagger e_{3,i} + (f_{1,i}^\dagger)^\dagger f_{1,i} + (f_{2,i}^\dagger)^\dagger f_{2,i} \left. \right] + V_5 \sum_i \left[A_{3,i}^\dagger (A_{1,i} + A_{2,i}) + B_{1,i}^\dagger (B_{2,i} + B_{3,i}) + C_{2,i}^\dagger (C_{1,i} \right. \\
& + C_{3,i}) + D_{3,i}^\dagger (D_{1,i} + D_{2,i}) + E_{1,i}^\dagger (E_{2,i} + E_{3,i}) + F_{2,i}^\dagger (F_{1,i} + F_{3,i}) \left. \right] + V_6 \sum_i \left[A_{1,i}^\dagger A_{2,i} + B_{2,i}^\dagger B_{3,i} + C_{1,i}^\dagger C_{3,i} \right. \\
& + D_{1,i}^\dagger D_{2,i} + E_{2,i}^\dagger E_{3,i} + F_{1,i}^\dagger F_{3,i} \left. \right] + V_7 \sum_i \left[(a_{2,i}^\dagger)^\dagger a_{3,i} + (a_{1,i}^\dagger)^\dagger a_{2,i} + (b_{2,i}^\dagger)^\dagger b_{3,i} + (b_{3,i}^\dagger)^\dagger b_{1,i} + (c_{1,i}^\dagger)^\dagger c_{2,i} \right. \\
& + (c_{3,i}^\dagger)^\dagger c_{1,i} + (d_{1,i}^\dagger)^\dagger d_{2,i} + (d_{2,i}^\dagger)^\dagger d_{3,i} + (e_{1,i}^\dagger)^\dagger e_{3,i} + (e_{2,i}^\dagger)^\dagger e_{3,i} + (f_{3,i}^\dagger)^\dagger f_{1,i} + (f_{1,i}^\dagger)^\dagger f_{2,i} \left. \right] + V_8 \sum_i \left[(a_{1,i}^\dagger)^\dagger a_{3,i} \right. \\
& + (a_{3,i}^\dagger)^\dagger a_{2,i} + (b_{1,i}^\dagger)^\dagger b_{3,i} + (b_{2,i}^\dagger)^\dagger b_{1,i} + (c_{3,i}^\dagger)^\dagger c_{2,i} + (c_{2,i}^\dagger)^\dagger c_{1,i} + (d_{3,i}^\dagger)^\dagger d_{2,i} + (d_{2,i}^\dagger)^\dagger d_{3,i} + (e_{1,i}^\dagger)^\dagger e_{2,i} + (e_{1,i}^\dagger)^\dagger e_{3,i} \\
& + (f_{2,i}^\dagger)^\dagger f_{1,i} + (f_{3,i}^\dagger)^\dagger f_{2,i} \left. \right] + V_9 \sum_i \left[(a_{1,i}^\dagger)^\dagger a_{2,i} + (a_{2,i}^\dagger)^\dagger a_{1,i} + (b_{1,i}^\dagger)^\dagger b_{2,i} + (b_{2,i}^\dagger)^\dagger b_{3,i} + (c_{3,i}^\dagger)^\dagger c_{1,i} + (c_{2,i}^\dagger)^\dagger c_{3,i} \right. \\
& + (d_{3,i}^\dagger)^\dagger d_{1,i} + (d_{1,i}^\dagger)^\dagger d_{2,i} + (e_{3,i}^\dagger)^\dagger e_{2,i} + (e_{1,i}^\dagger)^\dagger e_{2,i} + (f_{2,i}^\dagger)^\dagger f_{3,i} + (f_{3,i}^\dagger)^\dagger f_{1,i} \left. \right] + h.c. \tag{C4}
\end{aligned}$$

3. σ -tight-binding model for γ -graphyne

The labeling for γ -graphyne is shown in Fig. 15. The definition of the dominant NN hoppings (V_1, \dots, V_4) shown in Fig. 4(c) leads to

$$\begin{aligned}
H_{NN}^\gamma = & V_1 \sum_{\langle i,j \rangle} \left(A_{1,i}^\dagger F_{1,j} + A_{2,i}^\dagger B_{2,j} + C_{1,i}^\dagger D_{1,j} + C_{3,i}^\dagger B_{3,j} + E_{2,i}^\dagger D_{2,j} + E_{3,i}^\dagger F_{3,j} \right) + V_2 \sum_{\langle i,j \rangle} \left(A_{3,i}^\dagger a_{3,j} + B_{1,i}^\dagger b_{1,j} \right. \\
& + C_{2,i}^\dagger c_{2,j} + D_{3,i}^\dagger d_{3,j} + E_{1,i}^\dagger e_{1,j} + F_{2,i}^\dagger f_{2,j} \left. \right) + V_3 \sum_{\langle i,j \rangle} \left(a_{2,i}^\dagger d_{2,j} + b_{3,i}^\dagger e_{3,j} + c_{1,i}^\dagger f_{1,j} \right) + V_4 \sum_{\langle i,j \rangle} \left(a_{1,i}^\dagger d_{1,j} + b_{2,i}^\dagger e_{2,j} \right. \\
& \left. + c_{3,i}^\dagger f_{3,j} \right) + h.c. \tag{C5}
\end{aligned}$$

The onsite hoppings (V_5, V_6) and energies ($\varepsilon_1, \dots, \varepsilon_5$) yield

$$\begin{aligned}
H_{\text{onsite}}^\gamma = & \frac{\varepsilon_1}{2} \sum_i \left(A_{1,i}^\dagger A_{1,i} + A_{2,i}^\dagger A_{2,i} + B_{2,i}^\dagger B_{2,i} + B_{3,i}^\dagger B_{3,i} + C_{1,i}^\dagger C_{1,i} + C_{3,i}^\dagger C_{3,i} + D_{1,i}^\dagger D_{1,i} + D_{2,i}^\dagger D_{2,i} \right. \\
& + E_{2,i}^\dagger E_{2,i} + E_{3,i}^\dagger E_{3,i} + F_{1,i}^\dagger F_{1,i} + F_{3,i}^\dagger F_{3,i} \left. \right) + \frac{\varepsilon_2}{2} \sum_i \left(A_{3,i}^\dagger A_{3,i} + B_{1,i}^\dagger B_{1,i} + C_{2,i}^\dagger C_{2,i} + D_{3,i}^\dagger D_{3,i} + E_{1,i}^\dagger E_{1,i} \right. \\
& + F_{2,i}^\dagger F_{2,i} \left. \right) + \frac{\varepsilon_3}{2} \sum_i \left(a_{2,i}^\dagger a_{2,i} + b_{3,i}^\dagger b_{3,i} + c_{1,i}^\dagger c_{1,i} + d_{2,i}^\dagger d_{2,i} + e_{3,i}^\dagger e_{3,i} + f_{1,i}^\dagger f_{1,i} \right) + \frac{\varepsilon_4}{2} \sum_i \left(a_{3,i}^\dagger a_{3,i} + b_{1,i}^\dagger b_{1,i} \right. \\
& + c_{2,i}^\dagger c_{2,i} + d_{3,i}^\dagger d_{3,i} + e_{1,i}^\dagger e_{1,i} + f_{2,i}^\dagger f_{2,i} \left. \right) + \frac{\varepsilon_5}{2} \sum_i \left(a_{1,i}^\dagger a_{1,i} + b_{2,i}^\dagger b_{2,i} + c_{3,i}^\dagger c_{3,i} + d_{1,i}^\dagger d_{1,i} + e_{2,i}^\dagger e_{2,i} + f_{3,i}^\dagger f_{3,i} \right) \\
& + V_5 \sum_i \left[A_{3,i}^\dagger (A_{1,i} + A_{2,i}) + B_{1,i}^\dagger (B_{2,i} + B_{3,i}) + C_{2,i}^\dagger (C_{1,i} + C_{3,i}) + D_{3,i}^\dagger (D_{1,i} + D_{2,i}) + E_{1,i}^\dagger (E_{2,i} + E_{3,i}) \right. \\
& \left. + F_{2,i}^\dagger (F_{1,i} + F_{3,i}) \right] + V_6 \sum_i \left(A_{1,i}^\dagger A_{2,i} + B_{2,i}^\dagger B_{3,i} + C_{1,i}^\dagger C_{3,i} + D_{1,i}^\dagger D_{2,i} + E_{2,i}^\dagger E_{3,i} + F_{1,i}^\dagger F_{3,i} \right) + h.c. \quad (\text{C6})
\end{aligned}$$

Appendix D: Spin orbit coupling Hamiltonians

The SOC Hamiltonians $H_E^{z,\sigma}$ and $H_L^{z,\sigma}$ given in Eqs. (12) and (13), respectively, are written in terms of the p_x , p_y , and s orbitals. Since we would like to compute the effective SOC Hamiltonians based on Eq. (24), we need to rewrite Eqs. (12) and (13) in terms of the hybrid orbitals. In Table V we provide the convention we used for the change of basis.

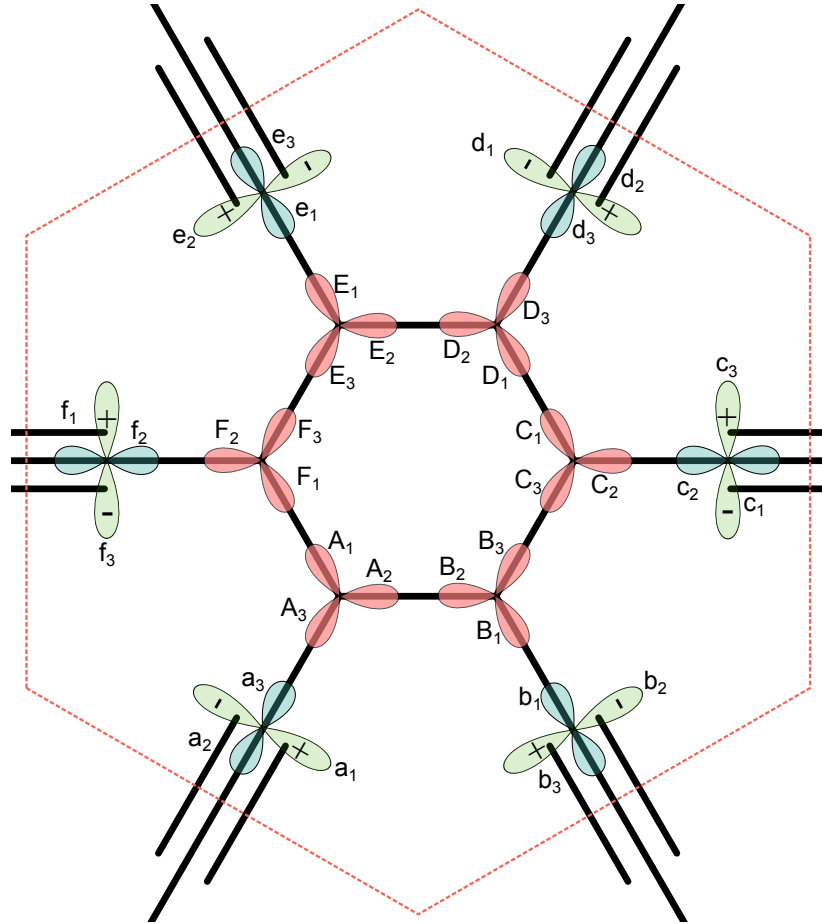


FIG. 15: (Color online) Labeling used for the γ -graphyne TB model.

1. α -graphyne

For α -graphyne, the Hamiltonians (12) and (13) rewritten in terms of the orbitals read

$$H_E^{z,\sigma} = \xi_{sp2} 3^{-1/2} \sum_i \left[A_i^\dagger (A_{1,i} + A_{2,i} + A_{3,i}) + B_i^\dagger (B_{1,i} + B_{2,i} + B_{3,i}) \right] + \xi_{sp1} 2^{-1/2} \sum_i \left[(a_i^1)^\dagger (a_{1,i}^1 + a_{3,i}^1) + (a_i^2)^\dagger (a_{1,i}^2 + a_{2,i}^2) + (a_i^3)^\dagger (a_{2,i}^3 + a_{3,i}^3) + (b_i^1)^\dagger (b_{1,i}^1 + b_{3,i}^1) + (b_i^2)^\dagger (b_{1,i}^2 + b_{2,i}^2) + (b_i^3)^\dagger (b_{2,i}^3 + b_{3,i}^3) \right], \quad (D1)$$

and

$$H_L^{z,\sigma} = i\xi_{p2} \sum_i \left[A_i^\dagger (2^{-1/2} \sigma_x + 6^{-1/2} \sigma_y) A_{1,i} + A_i^\dagger (-2/3)^{1/2} \sigma_y A_{2,i} + A_i^\dagger (-2^{-1/2} \sigma_x + 6^{-1/2} \sigma_y) A_{3,i} \right. \\ \left. B_i^\dagger (-2^{-1/2} \sigma_x - 6^{-1/2} \sigma_y) B_{1,i} + B_i^\dagger ((2/3)^{1/2} \sigma_y) B_{2,i} + B_i^\dagger (2^{-1/2} \sigma_x - 6^{-1/2} \sigma_y) B_{3,i} \right] \\ + i\xi_{p1} \sum_i \left[(a_i^1)^\dagger 2^{-1/2} (-\sqrt{3} \sigma_x / 2 - \sigma_y / 2) a_{1,i}^1 + (a_i^1)^\dagger (\sigma_x / 2 - \sqrt{3} \sigma_y / 2) a_{2,i}^1 + (a_i^1)^\dagger 2^{-1/2} (\sqrt{3} \sigma_x / 2 + \sigma_y / 2) a_{3,i}^1 \right. \\ + (a_i^2)^\dagger (-2^{-1/2} \sigma_y) a_{1,i}^2 + (a_i^2)^\dagger (2^{-1/2} \sigma_y) a_{2,i}^2 + (a_i^2)^\dagger (\sigma_x) a_{3,i}^2 \\ + (a_i^3)^\dagger (\sigma_x / 2 + \sqrt{3} \sigma_y / 2) a_{1,i}^3 + (a_i^3)^\dagger 2^{-1/2} (-\sqrt{3} \sigma_x / 2 + \sigma_y / 2) a_{2,i}^3 + (a_i^3)^\dagger 2^{-1/2} (\sqrt{3} \sigma_x / 2 - \sigma_y / 2) a_{3,i}^3 \\ + (b_i^1)^\dagger 2^{-1/2} (\sqrt{3} \sigma_x / 2 + \sigma_y / 2) b_{1,i}^1 + (b_i^1)^\dagger (\sigma_x / 2 - \sqrt{3} \sigma_y / 2) b_{2,i}^1 + (b_i^1)^\dagger 2^{-1/2} (-\sqrt{3} \sigma_x / 2 - \sigma_y / 2) b_{3,i}^1 \\ + (b_i^2)^\dagger 2^{-1/2} (\sigma_y) b_{1,i}^2 - (b_i^2)^\dagger 2^{-1/2} (\sigma_y) b_{2,i}^2 + (b_i^2)^\dagger (\sigma_x) b_{3,i}^2 \\ \left. + (b_i^3)^\dagger (\sigma_x / 2 + \sqrt{3} \sigma_y / 2) b_{1,i}^3 + (b_i^3)^\dagger 2^{-1/2} (\sqrt{3} \sigma_x / 2 - \sigma_y / 2) b_{2,i}^3 + (b_i^3)^\dagger 2^{-1/2} (-\sqrt{3} \sigma_x / 2 + \sigma_y / 2) b_{3,i}^3 \right] \quad (D2)$$

2. β -graphyne

Similarly, for β -graphyne we find

$$H_E^{z,\sigma} = \xi_{sp2} 3^{-1/2} \sum_i \left[A_i^\dagger (A_{1,i} + A_{2,i} + A_{3,i}) + B_i^\dagger (B_{1,i} + B_{2,i} + B_{3,i}) + C_i^\dagger (C_{1,i} + C_{2,i} + C_{3,i}) + D_i^\dagger (D_{1,i} + D_{2,i} \right. \\ \left. + D_{3,i}) + E_i^\dagger (E_{1,i} + E_{2,i} + E_{3,i}) + F_i^\dagger (F_{1,i} + F_{2,i} + F_{3,i}) \right] + \xi_{sp1} 2^{-1/2} \sum_i \left[(a_i^1)^\dagger (a_{2,i}^1 + a_{1,i}^1) + (a_i^2)^\dagger (a_{1,i}^2 + a_{3,i}^2) \right. \\ + (b_i^1)^\dagger (b_{2,i}^1 + b_{1,i}^1) + (b_i^2)^\dagger (b_{2,i}^2 + b_{3,i}^2) + (c_i^1)^\dagger (c_{1,i}^1 + c_{3,i}^1) + (c_i^2)^\dagger (c_{2,i}^2 + c_{3,i}^2) + (d_i^1)^\dagger (d_{1,i}^1 + d_{3,i}^1) \\ \left. + (d_i^2)^\dagger (d_{1,i}^2 + d_{2,i}^2) + (e_i^1)^\dagger (e_{3,i}^1 + e_{2,i}^1) + (e_i^2)^\dagger (e_{1,i}^2 + e_{2,i}^2) + (f_i^1)^\dagger (f_{2,i}^1 + f_{3,i}^1) + (f_i^2)^\dagger (f_{1,i}^2 + f_{3,i}^2) \right], \quad (D3)$$



















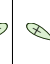


	sp^2						sp						p									
																						
s	$1/\sqrt{3}$	$1/\sqrt{3}$	$1/\sqrt{3}$	$1/\sqrt{3}$	$1/\sqrt{3}$	$1/\sqrt{3}$	$1/\sqrt{2}$	$1/\sqrt{2}$	$1/\sqrt{2}$	$1/\sqrt{2}$	$1/\sqrt{2}$	$1/\sqrt{2}$	$1/\sqrt{2}$	0	0	0	0	0	0	0	0	0
p_x	$1/\sqrt{6}$	$-\sqrt{2}/3$	$1/\sqrt{6}$	$-1/\sqrt{6}$	$\sqrt{2}/3$	$-1/\sqrt{6}$	$1/\sqrt{8}$	$-1/\sqrt{2}$	$1/\sqrt{8}$	$-1/\sqrt{8}$	$1/\sqrt{2}$	$-1/\sqrt{8}$	$-1/\sqrt{8}$	$-\sqrt{3}/2$	$\sqrt{3}/2$	0	$\sqrt{3}/2$	$-\sqrt{3}/2$	0	0	0	0
p_y	$1/\sqrt{2}$	0	$-1/\sqrt{2}$	$-1/\sqrt{2}$	0	$1/\sqrt{2}$	$\sqrt{3}/8$	0	$-\sqrt{3}/8$	$-\sqrt{3}/8$	0	$\sqrt{3}/8$	$-\sqrt{3}/8$	$-1/2$	$-1/2$	1	$1/2$	$1/2$	$-1/2$	$-1/2$	0	0

TABLE V: (Color online) Overlap between two sets of basis.

and

$$\begin{aligned}
H_L^{z,\sigma} = & i\xi_{p2} \sum_i \left[A_i^\dagger (2^{-1/2}\sigma_x + 6^{-1/2}\sigma_y) A_{1,i} + A_i^\dagger (-(2/3)^{1/2}\sigma_y) A_{2,i} + A_i^\dagger (-2^{-1/2}\sigma_x + 6^{-1/2}\sigma_y) A_{3,i} \right. \\
& + B_i^\dagger (-2^{-1/2}\sigma_x - 6^{-1/2}\sigma_y) B_{1,i} + B_i^\dagger ((2/3)^{1/2}\sigma_y) B_{2,i} + B_i^\dagger (2^{-1/2}\sigma_x - 6^{-1/2}\sigma_y) B_{3,i} \\
& + C_i^\dagger (2^{-1/2}\sigma_x + 6^{-1/2}\sigma_y) C_{1,i} + C_i^\dagger (-(2/3)^{1/2}\sigma_y) C_{2,i} + C_i^\dagger (-2^{-1/2}\sigma_x + 6^{-1/2}\sigma_y) C_{3,i} \\
& + D_i^\dagger (-2^{-1/2}\sigma_x - 6^{-1/2}\sigma_y) D_{1,i} + D_i^\dagger ((2/3)^{1/2}\sigma_y) D_{2,i} + D_i^\dagger (2^{-1/2}\sigma_x - 6^{-1/2}\sigma_y) D_{3,i} \\
& + E_i^\dagger (2^{-1/2}\sigma_x + 6^{-1/2}\sigma_y) E_{1,i} + E_i^\dagger (-(2/3)^{1/2}\sigma_y) E_{2,i} + E_i^\dagger (-2^{-1/2}\sigma_x + 6^{-1/2}\sigma_y) E_{3,i} \\
& \left. + F_i^\dagger (-2^{-1/2}\sigma_x - 6^{-1/2}\sigma_y) F_{1,i} + F_i^\dagger ((2/3)^{1/2}\sigma_y) F_{2,i} + F_i^\dagger (2^{-1/2}\sigma_x - 6^{-1/2}\sigma_y) F_{3,i} \right] \\
& + i\xi_{p1} \sum_i \left[(a_i^1)^\dagger (-2^{-1/2}\sigma_y) a_{1,i}^1 + (a_i^1)^\dagger (2^{-1/2}\sigma_y) a_{2,i}^1 + (a_i^1)^\dagger (\sigma_x) a_{3,i}^1 + (a_i^2)^\dagger 2^{-1/2} (-\sqrt{3}\sigma_x/2 - \sigma_y/2) a_{1,i}^2 \right. \\
& + (a_i^2)^\dagger (\sigma_x/2 - \sqrt{3}\sigma_y/2) a_{2,i}^2 + (a_i^2)^\dagger 2^{-1/2} (\sqrt{3}\sigma_x/2 + \sigma_y/2) a_{3,i}^2 + (b_i^1)^\dagger 2^{-1/2} \sigma_y b_{1,i}^1 - (b_i^1)^\dagger 2^{-1/2} \sigma_y b_{2,i}^1 \\
& + (b_i^1)^\dagger \sigma_x b_{3,i}^1 + (b_i^2)^\dagger (\sigma_x/2 + \sqrt{3}\sigma_y/2) b_{1,i}^2 + (b_i^2)^\dagger 2^{-1/2} (\sqrt{3}\sigma_x/2 - \sigma_y/2) b_{2,i}^2 - (b_i^2)^\dagger 2^{-1/2} (\sqrt{3}\sigma_x/2 - \sigma_y/2) b_{3,i}^2 \\
& + (c_i^2)^\dagger (\sigma_x/2 + \sqrt{3}\sigma_y/2) c_{1,i}^2 - (c_i^2)^\dagger 2^{-1/2} (\sqrt{3}\sigma_x/2 - \sigma_y/2) c_{2,i}^2 + (c_i^2)^\dagger 2^{-1/2} (\sqrt{3}\sigma_x/2 - \sigma_y/2) c_{3,i}^2 \\
& + (c_i^1)^\dagger 2^{-1/2} (-\sqrt{3}\sigma_x/2 - \sigma_y/2) c_{1,i}^1 - (c_i^1)^\dagger (\sigma_x/2 - \sqrt{3}\sigma_y/2) c_{2,i}^1 + (c_i^1)^\dagger 2^{-1/2} (\sqrt{3}\sigma_x/2 + \sigma_y/2) c_{3,i}^1 \\
& - (d_i^1)^\dagger 2^{-1/2} (-\sqrt{3}\sigma_x/2 - \sigma_y/2) d_{1,i}^1 - (d_i^1)^\dagger (\sigma_x/2 - \sqrt{3}\sigma_y/2) d_{2,i}^1 - (d_i^1)^\dagger 2^{-1/2} (\sqrt{3}\sigma_x/2 + \sigma_y/2) d_{3,i}^1 \\
& - (d_i^2)^\dagger (-2^{-1/2}\sigma_y) d_{1,i}^2 - (d_i^2)^\dagger (2^{-1/2}\sigma_y) d_{2,i}^2 - (d_i^2)^\dagger (\sigma_x) d_{3,i}^2 \\
& - (e_i^1)^\dagger (\sigma_x/2 + \sqrt{3}\sigma_y/2) e_{1,i}^1 - (e_i^1)^\dagger 2^{-1/2} (\sqrt{3}\sigma_x/2 - \sigma_y/2) e_{2,i}^1 + (e_i^1)^\dagger 2^{-1/2} (\sqrt{3}\sigma_x/2 - \sigma_y/2) e_{3,i}^1 \\
& - (e_i^2)^\dagger 2^{-1/2} \sigma_y e_{1,i}^2 + (e_i^2)^\dagger 2^{-1/2} \sigma_y e_{2,i}^2 - (e_i^2)^\dagger \sigma_x e_{3,i}^2 \\
& - (f_i^1)^\dagger (\sigma_x/2 + \sqrt{3}\sigma_y/2) f_{1,i}^1 + (f_i^1)^\dagger 2^{-1/2} (\sqrt{3}\sigma_x/2 - \sigma_y/2) f_{2,i}^1 - (f_i^1)^\dagger 2^{-1/2} (\sqrt{3}\sigma_x/2 - \sigma_y/2) f_{3,i}^1 \\
& \left. (f_i^2)^\dagger 2^{-1/2} (\sqrt{3}\sigma_x/2 + \sigma_y/2) f_{1,i}^2 + (f_i^2)^\dagger (\sigma_x/2 - \sqrt{3}\sigma_y/2) f_{2,i}^2 - (f_i^2)^\dagger 2^{-1/2} (\sqrt{3}\sigma_x/2 + \sigma_y/2) f_{3,i}^2 \right]. \tag{D4}
\end{aligned}$$

3. γ -graphyne

The SOC Hamiltonians for γ -graphyne are given by

$$\begin{aligned}
H_E^{z,\sigma} = & \xi_{sp2} 3^{-1/2} \sum_i \left[A_i^\dagger (A_{1,i} + A_{2,i} + A_{3,i}) + B_i^\dagger (B_{1,i} + B_{2,i} + B_{3,i}) + C_i^\dagger (C_{1,i} + C_{2,i} + C_{3,i}) + D_i^\dagger (D_{1,i} + D_{2,i} \right. \\
& \left. + D_{3,i}) + E_i^\dagger (E_{1,i} + E_{2,i} + E_{3,i}) + F_i^\dagger (F_{1,i} + F_{2,i} + F_{3,i}) \right] + \xi_{sp1} 2^{-1/2} \sum_i \left[a_i^\dagger (a_{2,i} + a_{3,i}) + b_i^\dagger (b_{1,i} + b_{3,i}) \right. \\
& \left. c_i^\dagger (c_{1,i} + c_{2,i}) + d_i (d_{2,i} + d_{3,i}) + e_i (e_{1,i} + e_{3,i}) + f_i (f_{1,i} + f_{2,i}) \right], \tag{D5}
\end{aligned}$$

and

$$\begin{aligned}
H_L^{z,\sigma} = & i\xi_{p2} \sum_i \left[A_i^\dagger (2^{-1/2}\sigma_x + 6^{-1/2}\sigma_y) A_{1,i} + A_i^\dagger (-(2/3)^{1/2}\sigma_y) A_{2,i} + A_i^\dagger (-2^{-1/2}\sigma_x + 6^{-1/2}\sigma_y) A_{3,i} \right. \\
& + B_i^\dagger (-2^{-1/2}\sigma_x - 6^{-1/2}\sigma_y) B_{1,i} + B_i^\dagger ((2/3)^{1/2}\sigma_y) B_{2,i} + B_i^\dagger (2^{-1/2}\sigma_x - 6^{-1/2}\sigma_y) B_{3,i} \\
& + C_i^\dagger (2^{-1/2}\sigma_x + 6^{-1/2}\sigma_y) C_{1,i} + C_i^\dagger (-(2/3)^{1/2}\sigma_y) C_{2,i} + C_i^\dagger (-2^{-1/2}\sigma_x + 6^{-1/2}\sigma_y) C_{3,i} \\
& + D_i^\dagger (-2^{-1/2}\sigma_x - 6^{-1/2}\sigma_y) D_{1,i} + D_i^\dagger ((2/3)^{1/2}\sigma_y) D_{2,i} + D_i^\dagger (2^{-1/2}\sigma_x - 6^{-1/2}\sigma_y) D_{3,i} \\
& + E_i^\dagger (2^{-1/2}\sigma_x + 6^{-1/2}\sigma_y) E_{1,i} + E_i^\dagger (-(2/3)^{1/2}\sigma_y) E_{2,i} + E_i^\dagger (-2^{-1/2}\sigma_x + 6^{-1/2}\sigma_y) E_{3,i} \\
& \left. + F_i^\dagger (-2^{-1/2}\sigma_x - 6^{-1/2}\sigma_y) F_{1,i} + F_i^\dagger ((2/3)^{1/2}\sigma_y) F_{2,i} + F_i^\dagger (2^{-1/2}\sigma_x - 6^{-1/2}\sigma_y) F_{3,i} \right] \\
& + i\xi_{p1} \sum_i \left[a_i^\dagger (-\sigma_x/2 - \sqrt{3}\sigma_y/2) a_{1,i} + a_i^\dagger 2^{-1/2} (-\sqrt{3}\sigma_x/2 + \sigma_y/2) a_{2,i} + a_i^\dagger 2^{-1/2} (\sqrt{3}\sigma_x/2 - \sigma_y/2) a_{3,i} \right. \\
& + b_i^\dagger 2^{-1/2} (\sqrt{3}\sigma_x/2 + \sigma_y/2) b_{1,i} + b_i^\dagger (-\sigma_x/2 + \sqrt{3}\sigma_y/2) b_{2,i} + b_i^\dagger 2^{-1/2} (-\sqrt{3}\sigma_x/2 - \sigma_y/2) b_{3,i} \\
& - c_i^\dagger 2^{-1/2} \sigma_y c_{1,i} + c_i^\dagger 2^{-1/2} \sigma_y c_{2,i} + c_i^\dagger \sigma_x c_{3,i} \\
& + d_i^\dagger (-\sigma_x/2 - \sqrt{3}\sigma_y/2) d_{1,i} + d_i^\dagger 2^{-1/2} (\sqrt{3}\sigma_x/2 - \sigma_y/2) d_{2,i} + d_i^\dagger 2^{-1/2} (-\sqrt{3}\sigma_x/2 + \sigma_y/2) d_{3,i} \\
& + e_i^\dagger 2^{-1/2} (-\sqrt{3}\sigma_x/2 - \sigma_y/2) e_{1,i} + e_i^\dagger (-\sigma_x/2 + \sqrt{3}\sigma_y/2) e_{2,i} + e_i^\dagger 2^{-1/2} (\sqrt{3}\sigma_x/2 + \sigma_y/2) e_{3,i} \\
& \left. + f_i^\dagger 2^{-1/2} \sigma_y f_{1,i} - f_i^\dagger 2^{-1/2} \sigma_y f_{2,i} + f_i^\dagger \sigma_x f_{3,i} \right] \tag{D6}
\end{aligned}$$

-
- ¹ A. H. Castro Neto, F. Guinea, N. M. R. Peres, K. S. Novoselov, and A. K. Geim, *Rev. Mod. Phys.* **81**, 109 (2009).
- ² C. L. Kane and E.J. Mele, *Phys. Rev. Lett.* **95**, 146802 (2005).
- ³ E. Kalesaki, C. Delerue, C. Morais Smith, W. Beugeling, G. Allan, and D. Vanmaekelbergh, *Phys. Rev. X* **4**, 011010 (2014).
- ⁴ M. Gibertini, A. Singha, V. Pellegrini, M. Polini, G. Vignale, A. Pinczuk, L. N. Pfeiffer, and K.W. West, *Phys. Rev. B* **79**, 241406 (2009).
- ⁵ K. K. Gomes, W. Mar, W. Ko, F. Guinea, and H. C. Manoharan, *Nature (London)* **483**, 306 (2012).
- ⁶ Y. Li, L. Xu, H. Liu, and Y. Li, *Chem. Soc. Rev.* **43**, 2572 (2014).
- ⁷ G. X. Li, Y. L. Li, H. B. Liu, Y. B. Guo, Y. J. Li, and D. B. Zhu, *Chem. Commun.* **46**, 3256 (2010).
- ⁸ R. H. Baughman, H. Eckhardt, M. Kertesz, *J. Chem. Phys.* **87**, 6687 (1987).
- ⁹ N. Narita, S. Nagai, S. Suzuki, and K. Nakao, *Phys. Rev. B* **58**, 11009 (1998).
- ¹⁰ K. Tahara, T. Yoshimura, M. Sonoda, Y. Tobe, and R. V. Williams, *J. Org. Chem.* **72**, 1437 (2007).
- ¹¹ J. Kang, J. Li, F. Wu, S.-S. Li, and J.-B. Xia, *J. Phys. Chem. C* **115**, 20466 (2011).
- ¹² Q. Yue, S. Chang, J. Kang, J. Tan, S. Qin, and J. Li, *J. Chem. Phys.* **136**, 244702 (2012).
- ¹³ S. W. Cranford and M. J. Buehler, *Carbon* **49**, 4111 (2011).
- ¹⁴ O. Leenaerts, B. Partoens, and F. M. Peeters, *App. Phys. Lett.* **103**, 013105 (2013).
- ¹⁵ D. Malko, C. Neiss, F. Vines, and A. Görling, *Phys. Rev. Lett.* **108**, 086804 (2012).
- ¹⁶ H. Huang, W. Duan, and Z. Liu, *New. J. Phys.* **15**, 023004 (2013).
- ¹⁷ J.-J. Zheng, X. Zhao, Y. Zhao, and X. Gao, *Sci. Reports* **3**, 1271 (2013).
- ¹⁸ B. G. Kim and H. J. Choi, *Phys. Rev. B* **86**, 115435 (2012).
- ¹⁹ J.-J. Zheng, X. Zhao, S. B. Zhang, and X. Gao, *J. Chem. Phys.* **138**, 244708 (2013).
- ²⁰ H. Zhang, M. Zhao, X. He, Z. Wang, X. Zhang, and X. Liu, *J. Phys. Chem. C* **115**, 8845 (2011).
- ²¹ H. J. Hwang, Y. Kwon, and H. Lee, *J. Phys. Chem. C* **116**, 20220 (2012).
- ²² J. He, S. Y. Ma, P. Zhou, C. X. Zhang, C. He, and L. Z. Sun, *J. Phys. Chem. C* **116**, 26313 (2012).
- ²³ M. Zhao, W. Dong, and A. Wang, *Sci. Reports* **3**, 3532 (2013).
- ²⁴ G. van Miert, C. Morais Smith, and V. Juričić, *Phys. Rev. B* **90**, 081406(R) (2014).
- ²⁵ Z. Liu, G. Yu, H. Yao, L. Liu, L. Jiang, and Y. Zheng, *New. J. Phys.* **14**, 113007 (2012).
- ²⁶ J.J. Sakurai, *Modern Quantum Mechanics*, 2nd ed. (Addison Wesley, Reading, MA, 2010).
- ²⁷ S. Kunschuh, M. Gmitra, and J. Fabian, *Phys. Rev. B* **82**, 245412 (2010).
- ²⁸ M. Zarea and N. Sandler, *Phys. Rev. B* **79**, 165442 (2009).
- ²⁹ R. van Gelderen and C. Morais Smith, *Phys. Rev. B* **81**, 125435 (2010).
- ³⁰ M. Gmitra, S. Kunschuh, C. Ertler, C. Ambrosch-Draxl, and J. Fabian, *Phys. Rev. B* **80**, 235431 (2009).
- ³¹ Samir Abdelouahed, A. Ernst, J. Henk, I. V. Maznichenko, and I. Mertig, *Phys. Rev. B* **82**, 125424 (2010).
- ³² J. C. Boettger and S. B. Trickey, *Phys. Rev. B* **75**, 121402(R) (2007).

³³ W. Han, R.K. Kawakami, M. Gmitra, and J. Fabian, Nature Nanotech. **9**, 794 (2014).

³⁴ S. Koghee, L.-K. Lim, M. O. Goerbig, and C. Morais

Smith, Phys. Rev. A **85**, 023637 (2012).